JGR Space Physics

RESEARCH ARTICLE
10.1029/2020JA028888

Key Points:

- We present a new multi-fluid magnetohydrodynamic model for Europa's plasma interaction, validated against data from the Galileo E4 and E14 flybys
- Our model estimates a thermal O^+ precipitation rate of (1.8–26)×10^{24} ions/s over the probable range of Jovian magnetospheric conditions
- The plasma interaction causes thermal magnetospheric plasma to precipitate on Europa's leading/downstream hemisphere

Correspondence to:
C. D. K. Harris,
cdha@umich.edu

Citation:
Harris, C. D. K., Jia, X., Slavin, J. A., Toth, G., Huang, Z., & Rubin, M. (2021). Multi-fluid MHD simulations of Europa's plasma interaction under different magnetospheric conditions. *Journal of Geophysical Research: Space Physics*, *126*, e2020JA028888. https://doi.org/10.1029/2020JA028888

Received 29 OCT 2020
Accepted 10 APR 2021

Multi-Fluid MHD Simulations of Europa's Plasma Interaction Under Different Magnetospheric Conditions

Camilla D. K. Harris[1], Xianzhe Jia[1], James A. Slavin[1], Gabor Toth[1], Zhenguang Huang[1], and Martin Rubin[2]

[1]Department of Climate and Space Sciences and Engineering, University of Michigan, Ann Arbor, MI, USA, [2]Physikalisches Institut, University of Bern, Bern, Switzerland

Abstract Europa hosts a periodically changing plasma interaction driven by the variations of Jupiter's magnetic field and magnetospheric plasma. We have developed a multi-fluid magnetohydrodynamic (MHD) model for Europa to characterize the global configuration of the plasma interaction with the moon and its tenuous atmosphere. The model solves the multi-fluid MHD equations for electrons and three ion fluids (Jupiter's magnetospheric O^+, as well as O^+ and O_2^+ originating from Europa's atmosphere) while incorporating sources and losses in the MHD equations due to electron impact and photo-ionization, charge exchange, recombination and other relevant collisional effects. Using input parameters constrained by the Galileo magnetic field and plasma observations, we first demonstrate the accuracy of our model by simulating the Galileo E4 and E14 flybys, which took place under different upstream conditions and sampled different regions of Europa's interaction. Our model produces 3D magnetic field and plasma bulk parameters that agree with and provide context for the flyby observations. We next present the results of a parameter study of Europa's plasma interaction at three different excursions from Jupiter's central plasma sheet, for three different global magnetospheric states, comprising nine steady-state simulations. By separately tracking multiple ion fluids, our MHD model allows us to quantify the access of the Jovian magnetospheric plasma to Europa's surface and determine how that access is affected by changing magnetospheric conditions. We find that the thermal magnetospheric O^+ precipitation rate ranges from (1.8–26) × 10^{24} ions/s, and that the precipitation rate increases with the density of the ambient magnetospheric plasma.

Plain Language Summary The moon Europa is embedded within Jupiter's magnetosphere, a region of space dominated by Jupiter's powerful magnetic field. The magnetosphere is filled with charged particles (plasma) which originate mainly from Jupiter's moon Io. Jupiter's magnetic field and plasma circulate throughout the magnetosphere. They flow around Europa and pile up as they approach Europa's ionosphere, a layer of plasma that surrounds the moon and partially shields the surface from the impact of Jupiter's magnetospheric plasma. Europa's ionosphere is generated from its atmosphere, which is in turn generated by surface sputtering, a process in which neutral particles are released when charged particles strike Europa's icy surface.

We have developed a computational model for Europa's space environment. We used the model to study how the changing conditions of Jupiter's magnetosphere affect the number and temperature of magnetospheric particles that are able to reach Europa's surface. With this result we can better understand the effect of conditions in Jupiter's magnetosphere on sputtering and, subsequently, on Europa's atmosphere. Understanding Europa's atmosphere and space environment will be critical for interpreting the observations of NASA's upcoming Europa Clipper mission.

1. Introduction

Europa orbits Jupiter at a mean distance of ~9.4 Jupiter radii on the outer edge of Jupiter's inner magnetosphere. In the reference frame moving with Europa, Jupiter completes a rotation every 11.1 h, and as the magnetospheric plasma and magnetic field corotate with the planet they overtake Europa from its trailing hemisphere with a velocity of ~100 km/s relative to Europa (e.g., Kivelson et al., 2004). As Jupiter's magnetic equator is tilted by ~10° from Europa's orbital plane the magnetosphere wobbles in Europa's frame of reference, causing the magnetic field and plasma populations that pass over Europa to vary periodically

with the 11.1 h synodic period of Jupiter's rotation. This time-varying flow of Jupiter's magnetospheric plasma and magnetic field leads to a periodically varying plasma interaction at Europa depending on its location relative to Jupiter's plasma sheet (e.g., Bagenal and Dols, 2020; Jia et al., 2010; Kivelson et al., 2009; Lipatov et al., 2013; Neubauer, 1999).

Europa hosts two global-scale conductive layers that shape the plasma interaction. The first is Europa's subsurface, briny ocean, which was discovered based on observations by the Galileo mission (1995–2003), and which makes Europa an exciting focus for the study of our solar system's ocean worlds. The Galileo magnetometer observed a roughly dipolar magnetic field near Europa that was consistent with an induced response to the 11.1 h periodic variation of the Jovian magnetic field at Europa (Kivelson et al., 2000). The strength and spatial form of the signal required the presence of a conducting subsurface ocean to support the eddy currents that generate the induced field (Khurana et al., 1998).

The second conductive layer is Europa's ionosphere. The ionospheric conductance is on the order of tens of siemens and therefore is too weak to produce a dipolar induced field of the same scale and magnitude as that of Europa's ocean (Neubauer et al., 1999; Zimmer et al., 2000). Additionally, while the time-varying magnetic fields of the plasma interaction induce small-scale magnetic fields of their own within the ionosphere, prior studies have demonstrated that these plasma-induced fields likely have little influence on the large-scale plasma interaction at Europa (Schilling et al., 2008). Nevertheless, the ionosphere is responsible for significant magnetic field and plasma perturbations. Kliore et al. (1997) determined, through radio occultation experiments conducted by the Galileo mission, that the ionospheric density varies considerably with space and time. The ionosphere is primarily composed of O_2^+ generated by electron impact ionization and photoionization of Europa's neutral O_2-dominated atmosphere. The atmosphere is, in turn, generated by the sputtering of charged particles from Jupiter's magnetosphere against Europa's icy surface. As the ionosphere interacts with the incident Jovian plasma to slow down the impinging magnetospheric plasma, and as the ambient magnetospheric plasma varies with the 11-hour synodic period of Jupiter's rotation, the feedback between the precipitating magnetospheric plasma and the generation of the atmosphere becomes complicated.

Europa's tenuous atmosphere is composed of H_2O, H_2, and O_2 (Hall et al., 1995, 1998), with O_2 being the dominant component (McGrath et al., 2009). Neutrals are liberated from Europa's icy surface by a number of processes, including sputtering, radiolysis, sublimation, and, potentially, water plumes (see a recent review by Plainaki et al., (2018)). Among these processes, sputtering by thermal magnetospheric ions (<100 eV) is expected to be more strongly affected by the plasma interaction (Johnson et al., 2009). Sputtering impacts by energetic ions tend to be uniformly distributed over Europa's surface (Breer et al., 2019; Paranicas et al., 2002; Pospieszalska and Johnson, 1989). However, sputtering by cooler, thermal plasma tends to be distributed asymmetrically, mainly impacting the trailing hemisphere as the corotating thermal population flows past Europa, leaving a wake with much reduced plasma density on the downstream side (Cassidy et al., 2013; Saur et al., 1998). Thermal particles sputter fewer neutrals per impact due to their lower energies, but the precipitation of thermal plasma to Europa's surface is much higher than that of energetic particles, potentially yielding a significant contribution to the total amount of sputtered neutrals (Cassidy et al., 2013; Vorburger and Wurz, 2018). The precipitation of thermal plasma is therefore an important factor in the yield of neutral O_2 and the subsequent generation of Europa's ionosphere. However, before the coupling between the neutral atmosphere and the plasma interaction can be studied, we must first characterize the precipitation of the thermal magnetospheric plasma. The spatial distribution and rate of thermal plasma precipitation onto Europa's surface is sensitive to the plasma interaction with Europa's ionosphere, which tends to divert the ambient flow of magnetospheric plasma around the moon, partially shielding the surface from direct impact. Understanding the precipitation of the thermal magnetospheric plasma onto Europa's surface and how it varies with the external conditions therefore requires self-consistent modeling of the different plasma populations present in the system and their coupling to the electromagnetic fields.

Several models for Europa's plasma interaction have considered the effects of magnetospheric thermal ions on the variability of the plasma interaction. Saur et al. (1998) determined that a plasma wake forms downstream of the moon due to diversion by the plasma interaction, and characterized how this diversion increases with the column density of the neutral atmosphere. Schilling et al. (2008) used a single-fluid magnetohydrodynamic (MHD) model to study the time-dependent interaction between Europa's atmosphere

and Jupiter's magnetosphere, with particular attention paid to the effects of induction. Rubin et al. (2015) introduced a two-ion-fluid MHD model that partially separated the plasma of Europa's ionosphere and Jupiter's magnetosphere to reveal the interaction of these distinct populations. Jia et al. (2018) subsequently used this model to identify signatures of a plume in Galileo magnetometer and plasma wave data. The results of Rubin et al. (2015) exhibited asymmetries on the anti- and sub-Jovian hemispheres in the distribution of plasma impinging on Europa's surface, and the authors presented maps of the flux of precipitating plasma onto the surface. However without complete separation of the magnetospheric and ionospheric plasma the precipitation rate of the thermal magnetospheric plasma could not be estimated.

To study the precipitation of thermal magnetospheric plasma onto Europa's surface we have extended and refined the model of Rubin et al. (2015) and Jia et al. (2018) to a three-ion-fluid model to solve for the bulk parameters of the thermal Jovian magnetospheric plasma separately from Europa's ionospheric plasma. We have fixed the neutral atmosphere and varied the external magnetospheric parameters of the model over multiple steady-state simulations to explore the parameter space of conditions that Europa experiences within the Jovian magnetosphere. We then measured the precipitation of the thermal magnetospheric plasma to the surface and characterized how properties of the magnetospheric plasma affect the spatial distribution and amount of precipitation.

In Section 2 we describe our multi-fluid MHD model for the plasma interaction and the updates we have made to the model of Rubin et al. (2015). We also review the parameter space of magnetospheric conditions at Europa that provided boundary conditions for the simulations. In Section 3 we present the results of 11 steady-state simulations: two corresponding to the Galileo E4 and E14 flybys, and a set of nine simulations representing Europa's plasma interaction at different magnetic latitudes and under different states of the Jovian magnetosphere. In Section 4 we discuss the precipitation of thermal plasma in these simulations. We summarize our results and findings in Section 5.

2. Methods

2.1. Model Description

Our model is based on that of Rubin et al. (2015), in which the authors used the multi-fluid capabilities of the BATS-R-US MHD code (Glocer et al., 2009; Toth et al., 2012) to self-consistently solve for the electromagnetic fields and bulk plasma properties of Europa's plasma interaction. Rubin et al. (2015) generated Europa's ionosphere from a static distribution of neutral O_2 by including mass, momentum, and pressure sources in the multi-fluid MHD equations for two ion fluids: a fluid representing O_2^+ originating in Europa's ionosphere, and a combined magnetospheric and ionospheric O^+ fluid. They also included an electron fluid. We have made improvements to the performance and accuracy of the model, expanded the simulation domain, increased the grid resolution, and used a more accurate scheme to solve the model equations. The most significant difference is our separation of magnetospheric O^+ ions from those generated by ionization of the atmosphere.

In our new model we solve the steady-state multi-fluid MHD equations for three ion fluids and one electron fluid so that we can separately track the O^+ ions of ionospheric and magnetospheric origin. The first ion fluid represents magnetospheric O^+ which streams past Europa from the upstream outer boundary. Though S^{2+} is also a significant component of the thermal magnetospheric plasma population at Europa's orbit (e.g., Kivelson et al., 2004), we did not include it as an additional fluid because the mass-to-charge ratio of S^{2+} is identical to that of O^+. As they also share bulk flow properties and both originate from the Io plasma torus, the two ion species would be redundant as MHD fluids.

The second and third ion fluids represent O_2^+ and O^+ ions that are generated from Europa's O_2-dominated atmosphere through electron impact ionization, photoionization, and charge exchange. These fluids together form Europa's ionosphere and an extended region of pick-up ions downstream. Ions may be lost as they leave the simulation's downstream outer boundary, by absorption to Europa's surface, or they may recombine with electrons to become neutrals. Separating the magnetospheric and ionospheric O+ ions is critical because their bulk properties (density, velocity, and temperature) are very different even in the same volume of the space plasma environment around Europa.

The 3-ion-fluid model retains most of the features of the previous 2-ion-fluid model described in Section 2 of Rubin et al. (2015). In the following sub-sections we describe the updates we have made to the numerical aspects of the simulation, the source terms, the boundary conditions, and the parameters of the neutral atmosphere. Cartesian coordinates and vector quantities are given in the Europa-centric EPhiO coordinate system, in which *X* points in the flow direction of Jupiter's corotating plasma, *Y* points toward Jupiter, and *Z* is parallel to Jupiter's spin axis.

2.1.1. Numerical Aspects

We solve the set of multi-fluid MHD equations (c.f. Equations 1–11 of Rubin et al., 2015) on a nonuniform spherical grid. The grid is logarithmically stretched in the radial dimension and block-adaptive grid refinement is used to increase the resolution in the near-Europa region. The simulation domain extends from R = 1 to 128 R_{Eu} (where Europa's mean radius R_{Eu} = 1,570 km). The smallest cell size near the simulation inner boundary just above Europa's surface is ~0.01 R_{Eu} = 15 km, while the largest cells at the outer boundary are ~10 R_{Eu} = 15,700 km in size. The equations are solved to obtain steady-state solutions using a second-order Linde scheme (for details of the scheme implementation in BATS-R-US see Toth et al., 2012).

2.1.2. Source Terms

Section 2.4 of Rubin et al. (2015) describes the implementation of source terms that model the effects of ionization, recombination, and charge exchange on the multi-fluid mass, momentum, and pressure MHD equations. In our new model, all three ion fluids experience recombination and charge exchange in the same manner as described by Rubin et al. (2015), with both O^+ fluids affected as described for the previous combined O^+ fluid.

However, we have updated the implementation of the ionization source terms. No magnetospheric O^+ is produced by ionization. Photoionization affects the O_2^+ and ionospheric O^+ fluids at the same rates specified by Rubin et al. (2015). Photoionization is applied uniformly over the whole simulation domain instead of being excluded from Europa's shadow as in Rubin et al. (2015). We found that the shadow made little difference in the steady state solution as the photoionization rate is 2 orders of magnitude lower than the electron impact ionization rate.

We have updated the calculation of the electron impact ionization rate to include ionization by suprathermal electrons from the Io plasma torus. We fix the temperature of the electron fluid to 20 eV, the typical temperature of thermal electrons (Bagenal and Dols, 2020), at the outer boundaries of the simulation domain. Perturbations to this temperature then develop self-consistently in the steady-state simulation according to the electron pressure equation (c.f. Equation 9 of Rubin et al., 2015), which includes the effects of the electron pressure source terms and field-aligned electron heat conduction. We use the method of Schilling (2006) and Rubin et al. (2015) to calculate the electron impact ionization rate for the ionospheric O_2^+ fluid based on the temperature of the thermal electron MHD fluid. We then add a uniform electron impact ionization rate due to the suprathermal population of electrons with low density (2 cm^{-3}) and high temperature (250 eV) that originate from the Io plasma torus (e.g., Bagenal and Dols, 2020), after the method of Saur et al. (1998).

In the Galileo flyby simulations, the average O_2^+ electron impact ionization rate within 200 km of Europa's surface is 1.1×10^{-6} s^{-1}. In the parameter study simulations, the average rate ranges from $(2.4–11.5) \times 10^{-6}$ s^{-1}. We prescribe the ionospheric O^+ electron impact ionization rate to be 10% of the O_2^+ rate (Rubin et al., 2015).

2.1.3. Boundary Conditions

Proper boundary and initial conditions are crucial to maintain stability as the simulation converges toward the steady-state solution. At the outer boundary we fix the plasma and magnetic field conditions according to Europa's location in Jupiter's magnetosphere at the moment represented by the steady state simulation. The method of selecting the outer boundary conditions for each simulation is described in Section 2.2, and the values of each parameter are given in Table 1.

Table 1
Simulation Boundary Conditions

	E4	E14	Case 1			Case 2			Case 3		
S3 Lon. [°]	157	184	19	76	110	19	76	110	19	76	110
Mag. Lat. [°]	6.5	9.2	−9.6	−5.6	−0.3	−9.6	−5.6	−0.3	−9.6	−5.6	−0.3
B_{Jx} [nT]	55.0	10.0	42.1	93.8	93.1	42.1	93.8	93.1	42.1	93.8	93.1
B_{Jy} [nT]	−173.0	−216.0	226.3	126.9	0	226.3	126.9	0	226.3	126.9	0
B_{Jz} [nT]	−412.0	−409.0	−400	−400	−400	−400	−400	−400	−400	−400	−400
M_x [nT]	−27.0	−5.0	−21.1	−46.9	−46.5	−21.1	−46.9	−46.5	−21.1	−46.9	−46.5
M_y [nT]	88.0	108.0	−113.2	−63.5	0	−113.2	−63.5	0	−113.2	−63.5	0
M_z [nT]	0	0	0	0	0	0	0	0	0	0	0
N_{O+} [cm^{-3}]	20.0	20.0	51.9	59.0	63.6	99.0	130.4	159.9	140.0	205.2	293.2
$U_{O+,x}$ [km/s]	100	100	100	100	100	100	100	100	100	100	100
T_{O+} [eV]	129.2	129.2	245.1	222.7	210.6	151.2	122.9	105.5	116.6	87.5	66.9
M_A	0.18	0.18	0.29	0.33	0.35	0.39	0.49	0.56	0.47	0.61	0.76

Magnetic field and plasma parameters for the outer boundary and induced dipole moment for each simulation.

The inner boundary represents Europa's surface, and we therefore treat the plasma properties and the magnetic field differently. We treat the velocity of the plasma fluids similarly to the method of Jia et al. (2009). We set each fluid velocity equal to the charge-averaged, field-perpendicular velocity

$$\vec{u}_{q,\perp} = \vec{u}_q - \frac{\vec{u_q} \cdot \vec{B}}{|\vec{B}|}\hat{b} \tag{1}$$

where b is the unit vector pointing along the local magnetic field B, and u_q is the charge-averaged velocity.

$$\vec{u}_q = \frac{\sum_s Z_s n_s \vec{u}_s}{\sum_s Z_s n_s} \tag{2}$$

here Z_s and n_s refer respectively to the charge state and number density of ion fluid s, where s indicates any of the three ion fluids described previously. If $u_{q,\perp}$ has a radially inward component, we impose a floating boundary condition such that the gradient of each fluid's density and pressure is zero, in effect modeling the absorption of plasma by Europa's surface. Where $u_{q,\perp}$ has a radially outward component we limit the density and pressure to very small values so that the inner boundary, which corresponds to Europa's icy surface, is not a significant source of plasma.

We specify conditions for the magnetic field such that there is no gradient across the inner boundary. The value of the magnetic field that is calculated by solving the magnetic induction equation (c.f. Equation 11 of Rubin et al., 2015) in the layer of cells adjacent to the surface is copied into the boundary cells. We prescribe Europa's induced magnetic field to be a dipole centered at the moon's origin with the moment directed in the XY plane. The direction and strength of the dipole moment correspond to the instantaneous induced field for each steady-state simulation; the method of calculating the induced field is described in Section 2.2 and the direction and strength of the prescribed induced field for each simulation are given in Table 1.

2.1.4. Neutral Atmosphere Model

We adopted the same functional form for the static neutral atmosphere as that used by Rubin et al. (2015) (c.f. Equation 22), which is also similar to those used in previous models for Europa's plasma interaction (e.g., Jia et al., 2018; Saur et al., 1998; Schilling et al., 2008). The choice of surface densities and scale heights is informed by the precedent set by previous models for the plasma interaction and updated with recent modeling of the neutral atmosphere using Monte Carlo methods (e.g., Oza et al., 2019; Plainaki et al., 2013; Teolis et al., 2017; Vorburger and Wurz, 2018).

Table 2
Mass-Loading and Charge Exchange Rates for the Ion Species in Each Simulation

	E4	E14	Case 1			Case 2			Case 3		
S3 Lon. [°]	157	184	19	76	110	19	76	110	19	76	110
Mag. Lat. [°]	6.5	9.2	−9.6	−5.6	−0.3	−9.6	−5.6	−0.3	−9.6	−5.6	−0.3
Mass-loading O_2^+ [kg/s]	3.1	3.1	4.1	4.6	4.8	5.7	7.2	8.1	7.1	9.6	12.1
Mass-loading O^+ [kg/s]	0.16	0.16	0.21	0.24	0.25	0.29	0.37	0.41	0.37	0.49	0.61
Charge exchange O_2^+ [kg/s]	5.13	5.13	6.66	7.29	7.44	9.19	11.45	13.11	11.54	15.97	21.52

The global mass-loading rates due to photoionization and electron impact ionization, and the resonant charge exchange rate between O_2^+ and O_2, in each simulation.

ith reference to the parameters of Equation 22 of Rubin et al. (2015), the neutral atmosphere for all the simulations in this study has a surface density of $n_0 = 2.5 \times 10^7$ cm^{-3}, and a scale height of $H_0 = 100$ km. We did not use the secondary population with low surface density and large scale height in these simulations (n_1 and H_1 in Rubin et al., 2015). Instead we increased the scale height of the primary population, in keeping with the results of Teolis et al., (2017). We also decreased the surface density. The minimum and maximum column densities of the atmosphere used in these simulations are 2.5×10^{14} cm^{-2} on the leading/downstream hemisphere and 7.5×10^{14} cm^{-2} at the apex of the trailing/upstream hemisphere. These values are within the range of observed O_2 column densities reported by Hall et al. (1998) of $(2.4–14) \times 10^{14}$ cm^{-2} based on whole-limb observations of Europa's oxygen atmosphere by the Hubble Space Telescope.

The density distribution of the neutral atmosphere controls the rate at which mass is loaded to the different ion fluids by the source terms discussed in Section 2.1.2. The global mass-loading rate due to photoionization and electron impact ionization of the neutral atmosphere in the Galileo E4 and E14 flyby simulations is 3.1 kg/s for the O_2^+ fluid and 0.16 kg/s for the ionospheric O^+. These rates are comparable to the estimate by Saur et al. (1998) of ∼7 kg/s for atmospheric loss due to ionization during the E4 flyby. For the set of nine parameter study simulations these rates range from 4.1 to 11.9 kg/s for O_2^+ and 0.21–0.60 kg/s for ionospheric O^+. The variation is caused by differences in the solutions for the electron temperature among the different simulations. All of these rates, and the global resonant charge exchange rates between O_2^+ and O_2, are calculated throughout the simulation domain according to the source terms discussed in Section 2.1.2. The total rates summed over the domain are summarized in Table 2.

2.2. Parameter Space for Magnetospheric Conditions

In this section we describe the methods by which the outer boundary plasma and magnetic field conditions, and the values for the induced field, were selected for each simulation. The values are summarized in Table 1. For the Galileo E4 and E14 flybys these values are informed by data collected by the Galileo spacecraft during each flyby. The Jovian background magnetic field (B_J) was determined by linearly fitting the flyby magnetometer data, excluding the perturbed values within ∼10 min of closest approach, and selecting the linear fit magnetic field values at closest approach. We used the magnetic moment values reported by Kivelson et al. (2000) for the E4 and E14 flybys. Paterson et al. (1999) reported an upstream total ion density of 20 cm^{-3} and upstream velocity of 100 km/s for the E4 flyby. In the absence of published data from the Galileo plasma analyzer (PLS) for the E14 flyby, we used the E4 flyby parameters.

To select the boundary conditions for the parameter study simulations we relied on the plasma models of Bagenal et al. (2015) and the Jupiter magnetic field model of Khurana et al. (1997) at Europa's orbit. We extracted the magnetic field and the plasma density at three System III longitudes chosen to represent Europa while it is deep in Jupiter's southern magnetic lobe (19°), transitioning from the southern lobe to the center of the plasma sheet (76°), and in the center of the plasma sheet crossing from the southern to the northern lobe (110°). The corresponding scenarios in the northern lobe would have differed only in the direction of the background magnetic field and the direction of the induced field. This would cause the magnetic features of the interaction to be mirrored about the XZ and YZ planes and we do not expect this to significantly

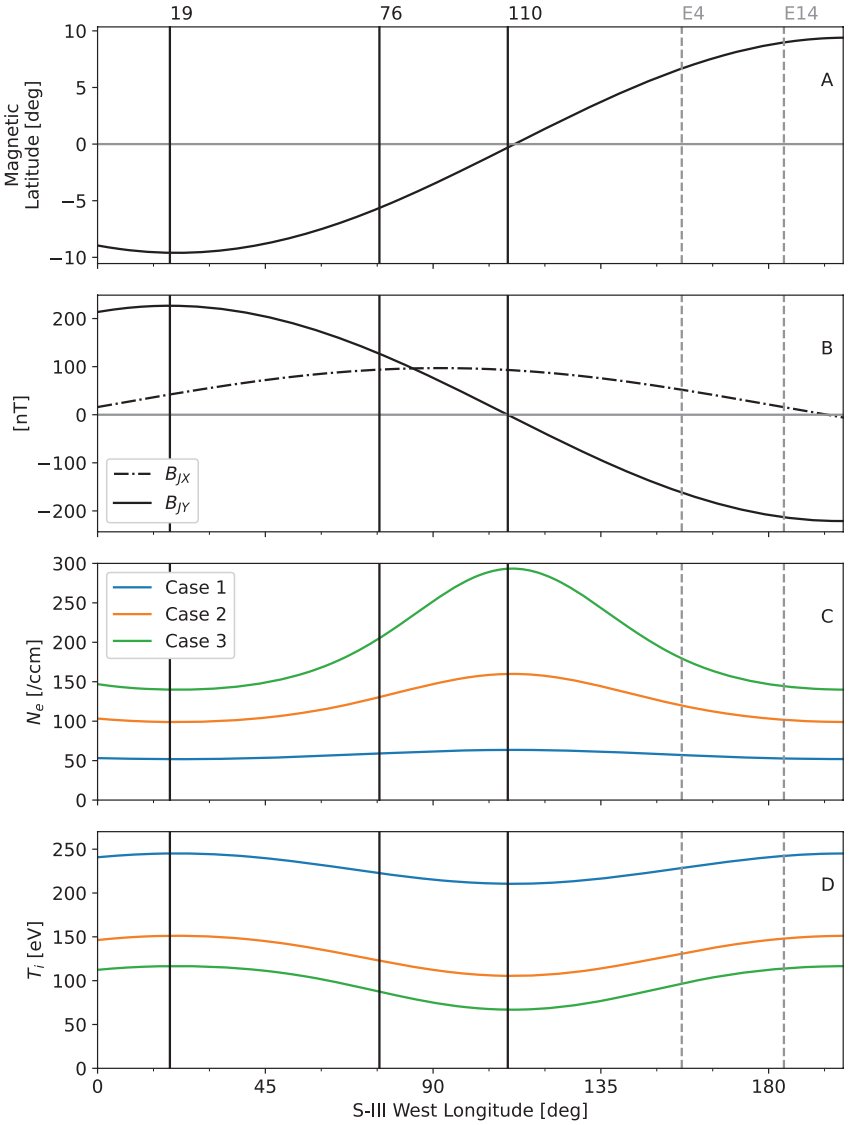

Figure 1. The range of parameters for the nine simulations at different magnetospheric conditions at Europa: (a) Magnetic latitude, (b) models for the Jovian magnetic field and (c and d) plasma conditions at Europa's orbit. Vertical black lines indicate the System III longitudes at which parameters for nine simulations were selected. In panels (c and d) the blue, orange, and green lines correspond respectively to the magnetospheric states 1, 2, and 3 of Bagenal et al. (2015). The vertical dashed gray lines indicate the longitudes of the Galileo E4 and E14 flybys.

affect the overall precipitation of plasma. We therefore limited the complexity of the study by omitting the northern cases. The ion temperatures for the parameter study simulations were determined using the power-law relationship between electron density and ion temperature that Bagenal et al. (2015) identified. As Bagenal et al. (2015) report three cases for the general state of the Jovian magnetosphere (Case 1: Low density and high temperature plasma; Case 2: Medium density and temperature plasma; Case 3: High density and low temperature plasma), this results in a total of nine simulations, as illustrated in Figure 1. To reduce the number of varying parameters we chose to fix the Z component of the ambient magnetic field (B_{Jz}) to −400 nT. We then calculated the magnetic moment of Europa's induced dipole assuming 100% efficient induction by the time-varying components of the magnetospheric magnetic field (B_{Jx} and B_{Jy}) such that M_X [nT] = $-B_{Jx}/2$ and M_Y [nT] = $-B_{Jy}/2$. Here the magnetic moment is given as a magnetic field vector with the equatorial strength of the magnetic field at Europa's surface as in Kivelson et al. (2000); in conventional units of A m^2 the moment is $4\pi R_{Eu}^3 M \mu_0$, where μ_0 is the magnetic permeability.

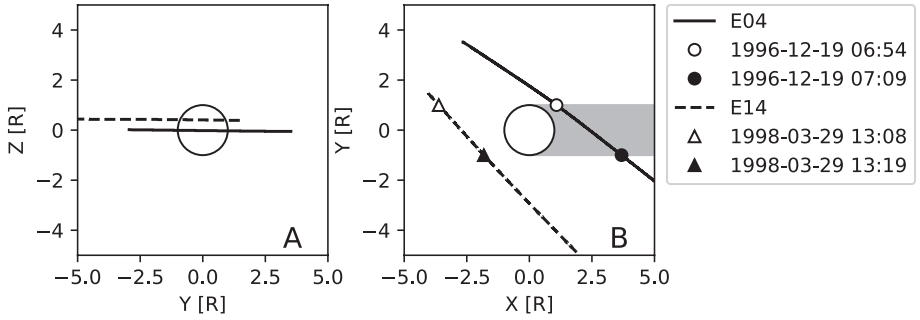

Figure 2. The E4 and E14 flyby trajectories in the (a) YZ and (b) XY planes. In Figure 2b symbols mark the points when the spacecraft entered and exited the region of Y = [1, −1]. The gray shaded region marks Europa's downstream geometric wake.

We set the speed of the corotating magnetospheric plasma relative to Europa to 100 km/s for all simulations. We also set the electron temperature to 20 eV for all the simulations, as previously described in Section 2.1.2.

We selected a relatively low density of the upstream plasma for the Galileo flyby simulations when compared to the upstream density in the parameter study simulations. For the nine simulations used in the parameter study, we set the upstream plasma density according to the electron densities reported by Bagenal et al. (2015), which were derived from the upper hybrid resonance frequencies as measured by the Galileo Plasma Waves Subsystem (PWS) (Kurth et al., 2001). As pointed out by Bagenal et al. (2015), the PWS-derived densities are generally higher than the PLS measurements. Since published plasma moments from PLS are available only for few Europa close flybys (e.g., E4), we based our choice of the upstream plasma densities for the parameter study on the PWS results (e.g., Bagenal et al., 2015; Kurth et al., 2001). As a result, the densities are consistently higher than the PLS density we used for the Galileo flyby simulations (E4 and E14).

The flyby simulations are intended to represent Europa's plasma interaction at the specific time of the corresponding flybys for the purpose of validating the model against the Galileo data set. The parameter study simulations do not represent any specific instant in time, but rather demonstrate the range of different responses of Europa's plasma interaction to the normal variations of the plasma and magnetic field in Jupiter's magnetosphere. The chosen input parameters span the known ranges for the Jovian magnetic field and plasma density and temperature at Europa's orbit (e.g., Bagenal et al., 2015; Bagenal and Dols 2020; Kivelson et al., 2009) and the associated Alfvén Mach numbers for all but the two most extreme simulations fall within the expected range of 0.08–0.59 (Kivelson et al., 2004). Therefore, while the selected upstream plasma densities do differ systematically between the flyby and the parameter study simulations, the parameter study simulations provide a realistic representation of the variability of the plasma interaction.

3. Results

3.1. Model Validation by Data-Model Comparison with the Galileo E4 and E14 Flybys

To demonstrate the ability of our model to simulate the plasma interaction, we first present two simulations representing the Galileo E4 and E14 flybys. The E4 flyby was simulated previously by Rubin et al. (2015), and our results demonstrate that the present model performs at least as well as the previous model. As illustrated in Figure 2, the E4 flyby passed through Europa's plasma wake on the downstream side, while the E14 flyby passed through the upstream part of the plasma interaction. Additionally, the E14 flyby occurred while Europa was deeper in Jupiter's magnetic lobe. Therefore, these two flybys sampled the upstream and downstream features of the interaction under different driving magnetic field conditions.

The E4 flyby occurred on 1996-12-19 from 06:54 to 07:09 UT. The spacecraft passed through Europa's wake with closest approach distance of 0.4 R_{Eu}. Europa was located in the northern lobe of Jupiter's magnetosphere, above the plasma sheet at 6.5° magnetic latitude (Kivelson et al., 2000). Figure 3 compares the magnetic fields observed by the Galileo magnetometer with the model results extracted from the E4 simulation along the spacecraft trajectory. Figure 3 illustrates that during the E4 flyby the X and Y components of the

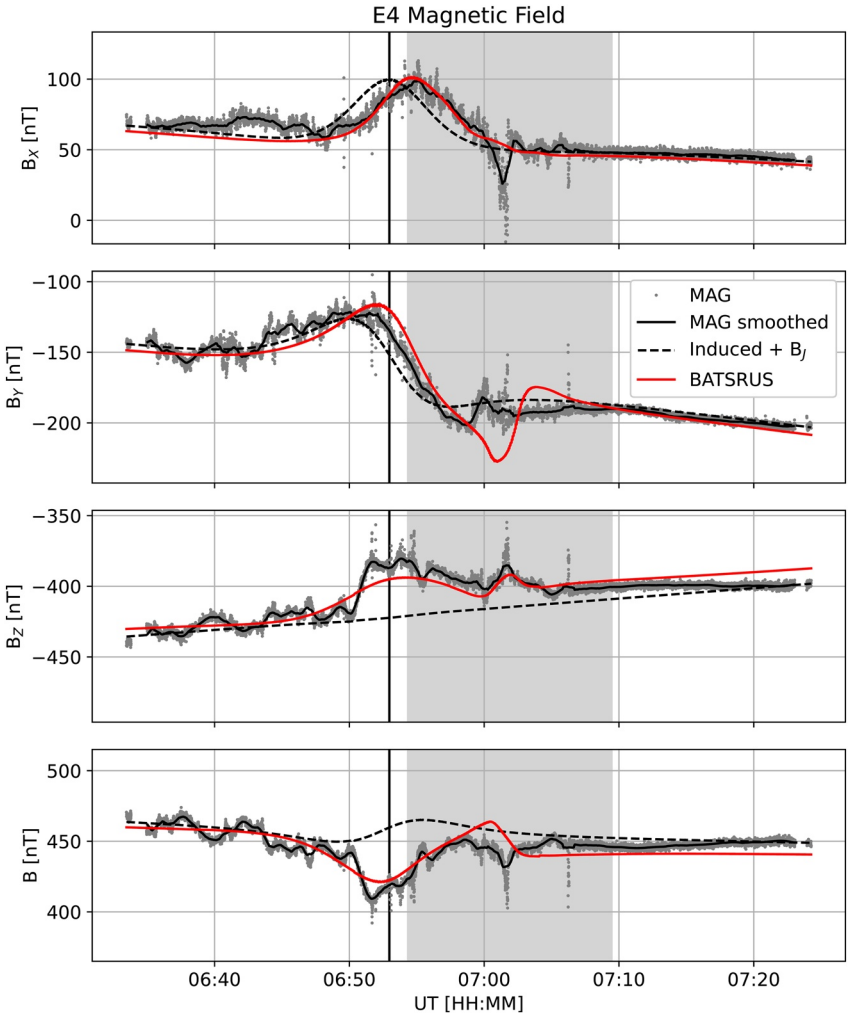

Figure 3. Comparison of simulated magnetic fields to the Galileo magnetometer observations for the E4 flyby. Gray dots indicate the Galileo magnetometer data, while the solid black line shows the data smoothed with a rolling boxcar average of 50 s. The black dashed line indicates the sum of the dipole representing the induced field background Jovian magnetic field. The red solid line gives the simulated magnetic field. The vertical black line indicates the time of closest approach, while the gray shaded area spans the time that the spacecraft spent in the region of $-1 < Y < 1$.

magnetic field were dominated by Europa's induced magnetic field. Both components vary smoothly near closest approach, then return to their background values as the spacecraft exited the wake. In the center of the wake the model B_Y field (Figure 3, second panel) dips, then peaks before exiting the wake. This could be a distortion of a similar feature observed in the magnetometer B_y data, where there is a shallow dip followed by a peak of ~20 nT at 07:00 UT. In the Z component of the magnetic field there is very little contribution from the induced field, as it is represented by a dipole moment directed in the XY plane and the E4 flyby was nearly confined to the XY plane. Therefore, the perturbations in B_z are caused predominantly by the magnetic fields associated with the plasma interaction. The Galileo magnetometer observed a weakening of the Z component and the overall magnitude of the magnetic field just before closest approach, then a slow return to background values as the spacecraft passed through the wake and moved away from the moon. Our simulation shows the same change in B_z including the depletion in magnetic field strength near closest approach and the same recovery through Europa's plasma wake.

Though the magnetic field weakened near closest approach, Figure 4 shows that the density of plasma was enhanced during the E4 flyby. The PLS reports that while the number density of the upstream magnetospheric plasma was 20 cm^{-3}, the density began to rise just prior to closest approach and in the center of

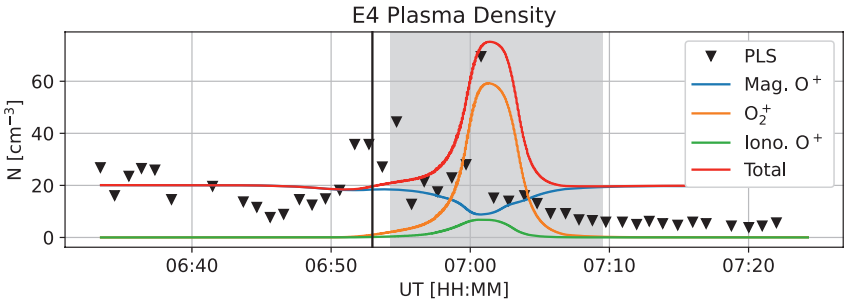

Figure 4. Comparison of the simulated plasma densities to the Galileo PLS total plasma density observations for the E4 flyby. The observed PLS densities are given by black triangles while the color curves show the number density of the Jovian magnetospheric O^+ (blue), $O_2{}^+$ (orange), ionospheric O^+ (green), and the total ion number density (red) which is equivalent to the electron density. Other annotations are as described for Figure 3. PLS, Galileo plasma analyzer.

Europa's wake the plasma density abruptly increased by a factor of three. Our simulation exhibits similar features. Prior to closest approach the density begins to increase due to the presence of $O_2{}^+$, though the increase is slower and less dramatic in the model. We also observe that the modeled plasma density peaks in the center of the wake, though the modeled peak is wider than the single data point of the PLS measurements. Paterson et al. (1999) note that this peak is likely significant despite the single data point due to a simultaneous increase in temperature. By separately tracking different ion fluids in the simulation, our multi-fluid model shows that the ionospheric species are responsible for this density increase. As some of the ambient magnetospheric O^+ is absorbed by Europa on the upstream side, this leads to a depletion of magnetospheric O^+ in Europa's wake region relative to the upstream densities. The ionospheric fluids are abundant near Europa's surface where the neutral atmosphere is densest, so these fluids are transported downstream to fill the wake and are then observed on the flyby trajectory as shown in Figure 4, causing the peak in number density.

The time of closest approach for the E4 flyby occurred as the spacecraft was moving from the flank of the interaction region to the sub-Jovian edge of the wake. Figure 5 shows that the X component of the plasma velocity was enhanced as the spacecraft passed through the fast flows on the flank, then decreased and returned to the ambient values through the wake. Our simulation has accurately modeled the enhanced speeds on the flank. However, there is a systematic offset in the Y component of the velocity between our simulation and the data, with the PLS seeing more positive flow in the *Y* direction by about 20–30 km/s compared to the simulation.

On 1998-3-29 from 13:05 to 13:40 UT the Galileo spacecraft conducted the E14 flyby across the upstream part of Europa's plasma interaction, as shown in Figure 2. The distance of closest approach was 1.05 R_{Eu}, and Europa was positioned deeper in Jupiter's northern lobe at 9.2° magnetic latitude (Kivelson et al., 2000). Figure 6 shows a good agreement to within a few nT between the simulated magnetic fields and the observations from the magnetometer. Figure 6 shows that, as for the E4 flyby, the variations of the *X* and Y components of the magnetic field are dominated by the induced magnetic field, but the model accurately simulates the magnetic effects of the plasma interaction, closing the gap between the induced field and the data. Similarly, in the *Z* component there is good agreement between the data and the model as the spacecraft passes through the enhancement of magnetic field strength upstream of the moon, caused by the slowing of the plasma flow and piling-up of magnetic field lines on the upstream side of the interaction. While the upstream pile-up of magnetic field is roughly symmetric about the XZ plane, the E14 flyby trajectory passes through the -Y side of the interaction, causing the spacecraft to observe the peak in magnetic field strength not when the spacecraft passes through Y = 0 (the center of the gray span in Figure 6), but later, closer to the time of the spacecraft's closest approach.

In Figures 7 and 8 we show the E14 simulated density and velocity, though no published PLS plasma moments are available for this flyby. The closest approach of the E14 flyby occurred at 1.05 R_{Eu} from the surface on the upstream side, more than twice as far as the distance of closest approach for the E4 flyby. At these distances, the densities of the ionospheric fluids in the simulation are negligibly small along the spacecraft trajectory ($\sim 2 \times 10^{-3}$ cm^{-3}), and, therefore, we omit the densities of the ionospheric fluids in Figure 7.

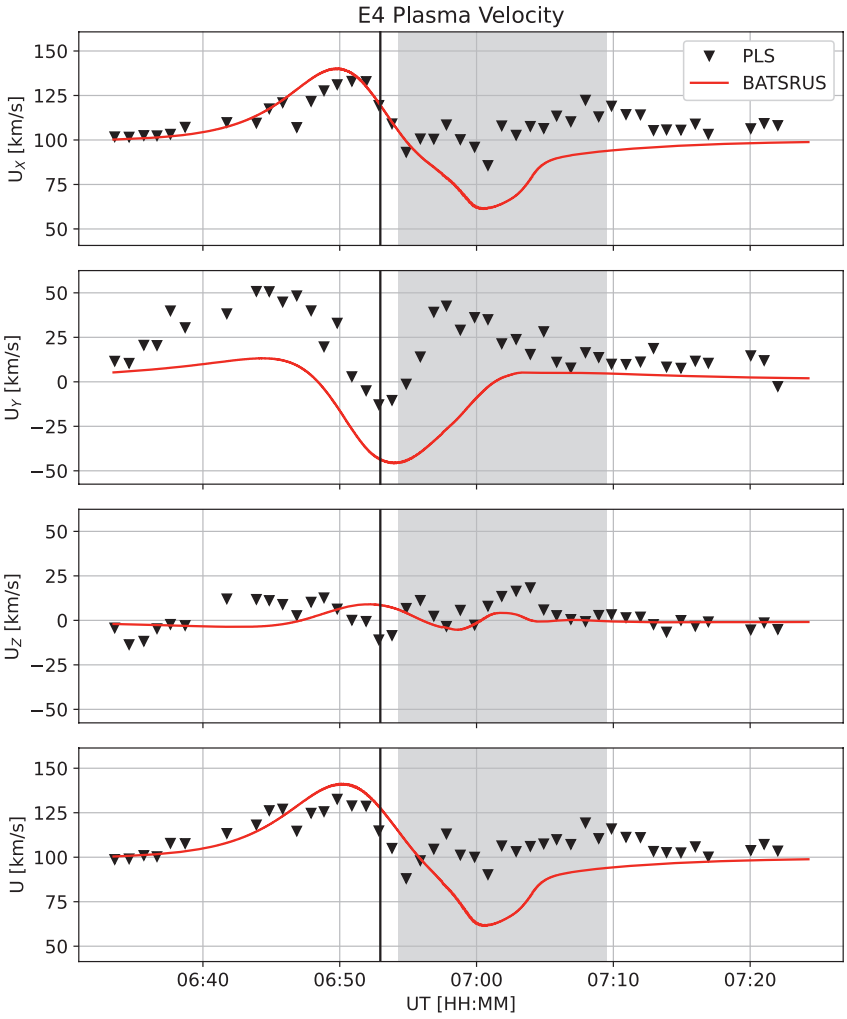

Figure 5. Comparison of the simulated charge-averaged fluid velocity (red curve) to the Galileo PLS total plasma velocity observations for the E4 flyby (Paterson et al., 1999) (black triangles). Other annotations are as described for Figure 3. PLS, Galileo plasma analyzer.

However, we see that there is a slight enhancement in the total number density due to the magnetospheric O^+ fluid on the upstream side of the plasma interaction, again caused by the slowing-down of the flow (Figure 8) and piling-up of the magnetic field (Figure 6) ahead of the moon. The trajectory then proceeds through the anti-Jovian flank, where the speed increases, before moving away from Europa. The density and velocity have returned to their ambient values by the end of the flyby.

The good data-model comparison between our simulations and the Galileo observations for these flybys demonstrates that our model can accurately represent the large-scale features of the plasma interaction, and can contend with the changing conditions throughout Jupiter's magnetosphere.

3.2. Parameter Study of Different Magnetospheric Conditions

To study the response of the plasma interaction to the variable driving conditions at Europa through one planetary rotation, we have conducted nine simulations. Each simulation represents the plasma interaction at one of three representative locations relative to the center of Jupiter's plasma sheet (lobe, transition, and plasma sheet), with 3 different possible cases of the magnetospheric state after Bagenal et al. (2015) (low density Case 1, medium density Case 2, and high density Case 3). See Table 1 for the detailed input parameters for the simulations. Figure 9 shows the *X* component of the charge-averaged velocity (Equation 2) in

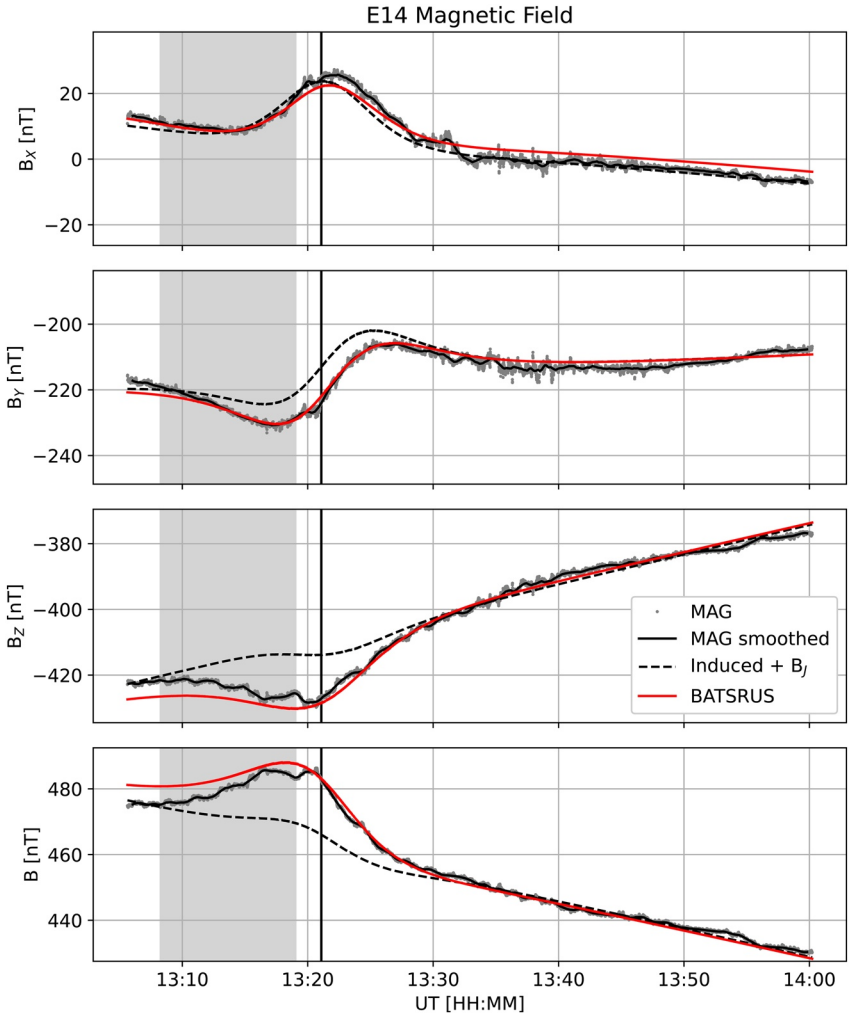

Figure 6. Comparison of simulated magnetic fields to the Galileo magnetometer observations for the E14 flyby. Annotations are as described for Figure 3.

the XZ plane for each simulation. The XZ plane intersects the Alfvén wing structure of the plasma interaction (Neubauer, 1998), though in the lobe and transitional magnetic configurations (left and center columns of Figure 9) there is a nonzero Y component to the background magnetic field, which causes the Alfvén wings to tilt out of the XZ plane at approximately the same angle as the YZ component of the background magnetic field. This tilt causes the fast flows of plasma that are diverted to either side of the Alfvén wings to pass through the XZ plane and appear in Figure 9. Within the Alfvén wings the plasma velocity slows as the

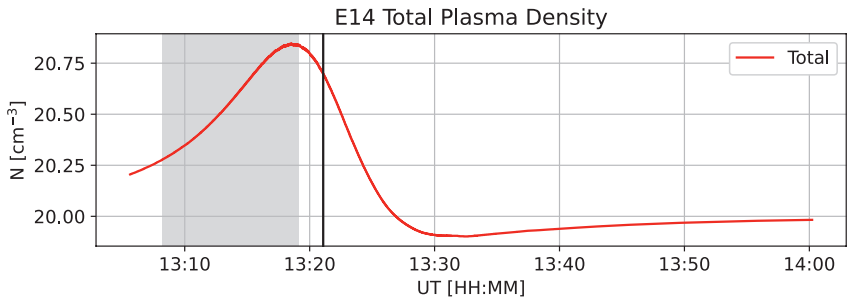

Figure 7. Simulated plasma density for the E14 flyby. Published PLS densities are not available for this flyby. Annotations are as described for Figure 4. PLS, Galileo plasma analyzer.

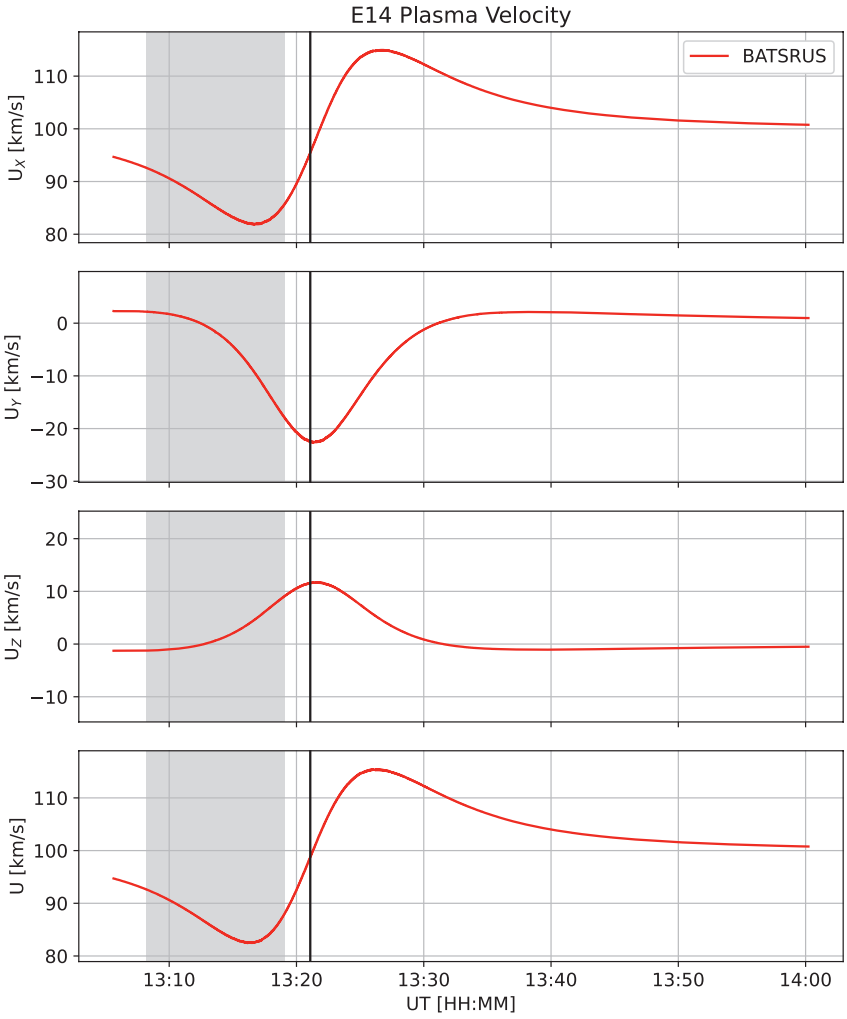

Figure 8. Simulated charge-averaged plasma velocity for the E14 flyby. Published PLS velocities are not available for this flyby. Annotations are as described for Figure 5. PLS, Galileo plasma analyzer.

field lines interact with Europa's ionosphere and induced field (Neubauer, 1998; Volwerk et al., 2007). It can be clearly seen in the plasma sheet simulations (right column of Figure 9) that the angle of the Alfvén wing characteristics with respect to the ambient magnetic field increases from Case 1 to Case 3 as the density of the ambient plasma, and thus the corresponding Alfvénic Mach number, increases.

To illustrate the general features of the plasma interaction as predicted by our multi-fluid simulations, we show the equatorial plane of the Case 1, plasma sheet simulation in Figures 10 and 11. We have focused on this simulation since the Jovian magnetic field is confined to the XZ plane and the Alfvénic Mach number of the ambient flow (0.35) is close to the average Mach number expected for Europa's plasma interaction (Kivelson et al., 2004).

In Figure 10 we show the density of each ion fluid and the electrons. We see that upstream of the interaction (-X side) the magnetospheric O^+ density increases as magnetic field lines pile up due to the interaction with the cool, dense ionosphere close to Europa's surface. Near the surface O_2^+ and ionospheric O^+ are generated mainly by electron impact ionization of the neutral atmosphere, so their densities are high and the impinging magnetospheric O^+ is partially diverted. On the downstream side of the interaction a wake has formed. The wake is relatively depleted of magnetospheric O^+ and populated with the ionospheric fluids, as we saw previously in Figure 4 for the E4 flyby.

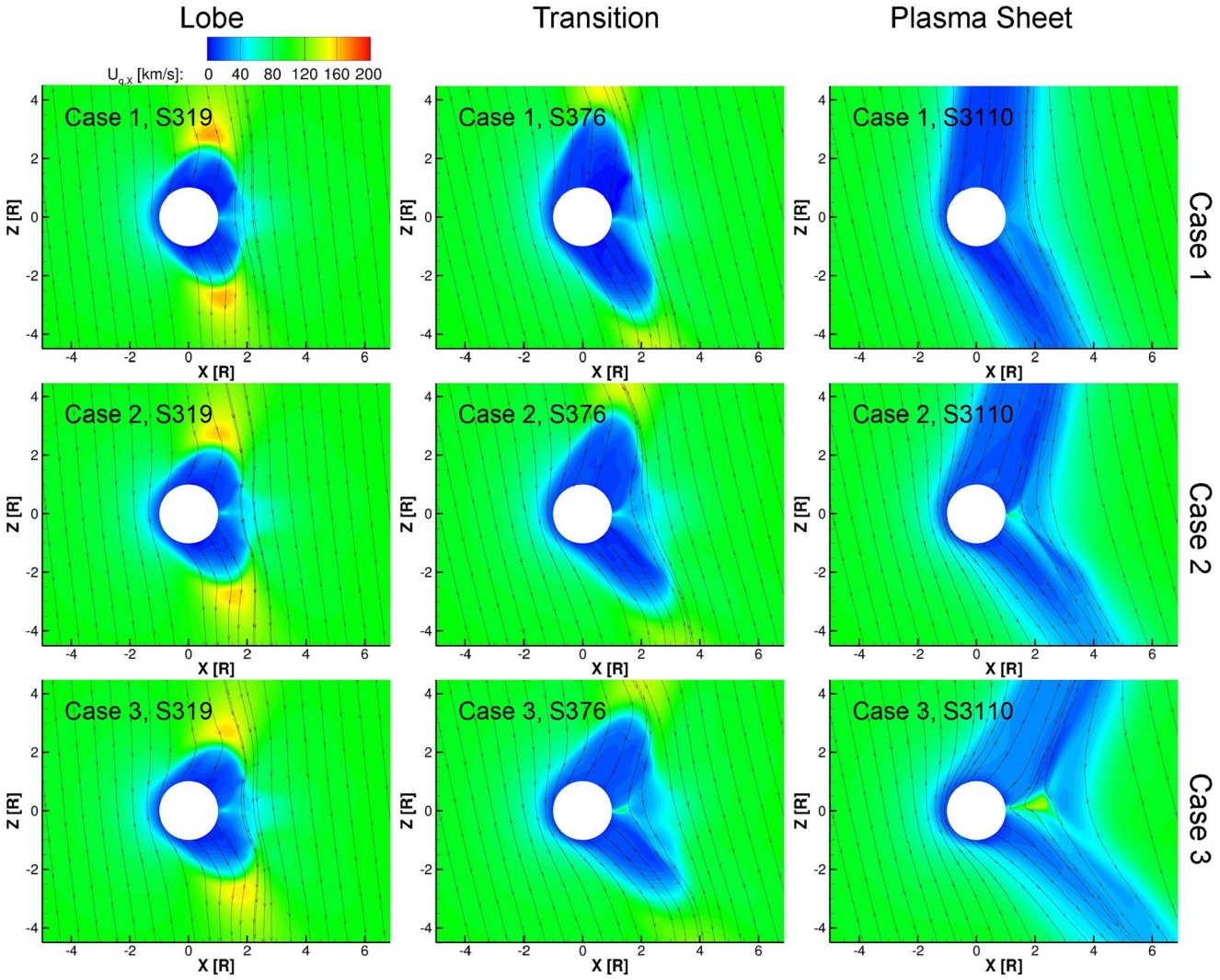

Figure 9. Contours of u_{qx} overlaid with B_{XZ} field lines in the Y = 0 plane for each of the 9 parameter study simulations.

Figure 11 exhibits sub- and anti-Jovian asymmetries in the X components of the fluid velocities. The interaction is approximately symmetric close to Europa's surface, in the upstream pile-up region, and in the wake. However, on the flanks the magnetospheric O^+ flows faster around the sub-Jovian side of the interaction while the O_2^+ and ionospheric O^+ flow faster around the anti-Jovian sides. The same asymmetry was observed by Rubin et al. (2015) in their simulation of the E4 flyby. Rubin et al. (2014) investigated similar features in a multi-fluid MHD model for comet-solar wind interactions; while a fluid model is not capable of simulating the full kinetics of particle gyration, they found that multi-fluid MHD does reproduce the separation of the bulk flows of the fluids. In our model, when new ions are introduced by ionization of Europa's extended atmosphere, they are initially cold and immobile. However, the magnetic field flows through the plasma interaction with the charge-averaged velocity, which is dominated by the flow of the magnetospheric O^+ fluid. Therefore, the ionospheric ions have velocity relative to the magnetic field. They are imparted with anti-Jovian directed velocity by the Lorenz force, as can be seen most clearly in Figure 11c where the O_2^+ streamlines preferentially lean to the -Y direction. Over the flanks the velocity streamlines are compressed due to diversion of the plasma away from the surface, causing the speed to increase. Because the O_2^+ fluid has been preferentially diverted in the -Y direction the compression is more severe on the anti-Jovian flank, causing the speed to increase more relative to the sub-Jovian flank. This results in the asymmetries seen in Figure 11.

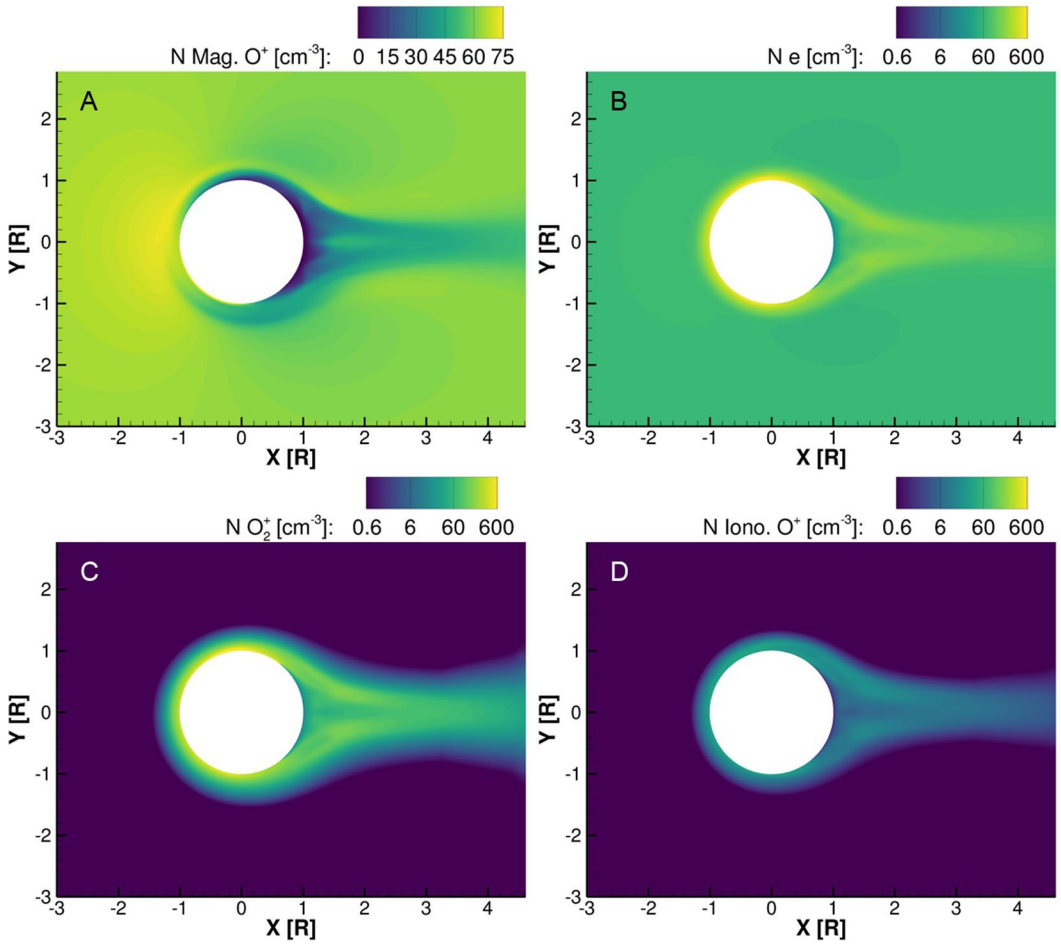

Figure 10. Simulated number densities on a logarithmic scale in the equatorial plane of the case 1, plasma sheet simulation for (a) Jupiter's magnetospheric O^+ ions, (b) electrons, (c) O_2^+ ions, and (d) ionospheric O^+ ions.

Figure 12 presents altitudinal profiles of the density of the magnetospheric plasma and of Europa's ionosphere along the upstream line (-X axis) as it was self-consistently generated in each simulation. In Figure 12a the density of the magnetospheric plasma peaks upstream of the moon where the magnetic field lines, and the plasma tied to them, have piled up in front of the ionosphere. The density returns to near-ambient values by ~6,240 km (4 R_{Eu}). Figure 12b shows that the density of Europa's ionosphere peaks near Europa's surface where the plasma is generated by ionization of the neutral atmosphere, then falls off with distance. For the 11 simulations presented in this study, the peak ionospheric plasma density near Europa's surface ranges from ~300 to 2,000 cm^{-3}, which falls within the observed range of ionospheric densities from the Galileo radio occultation experiment (Kliore et al., 1997; McGrath et al., 2009). In Figure 13 we show the integrated column density of the altitudinal profiles in Figure 12b, plotted versus the upstream magnetospheric plasma density for each simulation. The Case 3 (high density) simulations produced the densest ionospheres across each location, while the Case 1 (low density) simulations produced the most tenuous ionospheres. Within each case the plasma sheet simulation produced the densest ionosphere. In the E4 and E14 flyby simulations the upstream magnetospheric plasma density was set to 20 cm^{-3} as determined from the Galileo PLS data, and as such produced the most tenuous ionospheres of the whole set.

Figure 13 demonstrates that the column density of the ionosphere in each simulation increases with the density of the ambient magnetospheric plasma. The ionospheric plasma is generated mainly by electron impact ionization of the neutral atmosphere, with a minor contribution from photo-ionization. Therefore, the amount of plasma produced depends on the local density of the neutral atmosphere and, to a large extent, the local electron impact ionization rate. The neutral atmosphere has been purposefully held constant in all

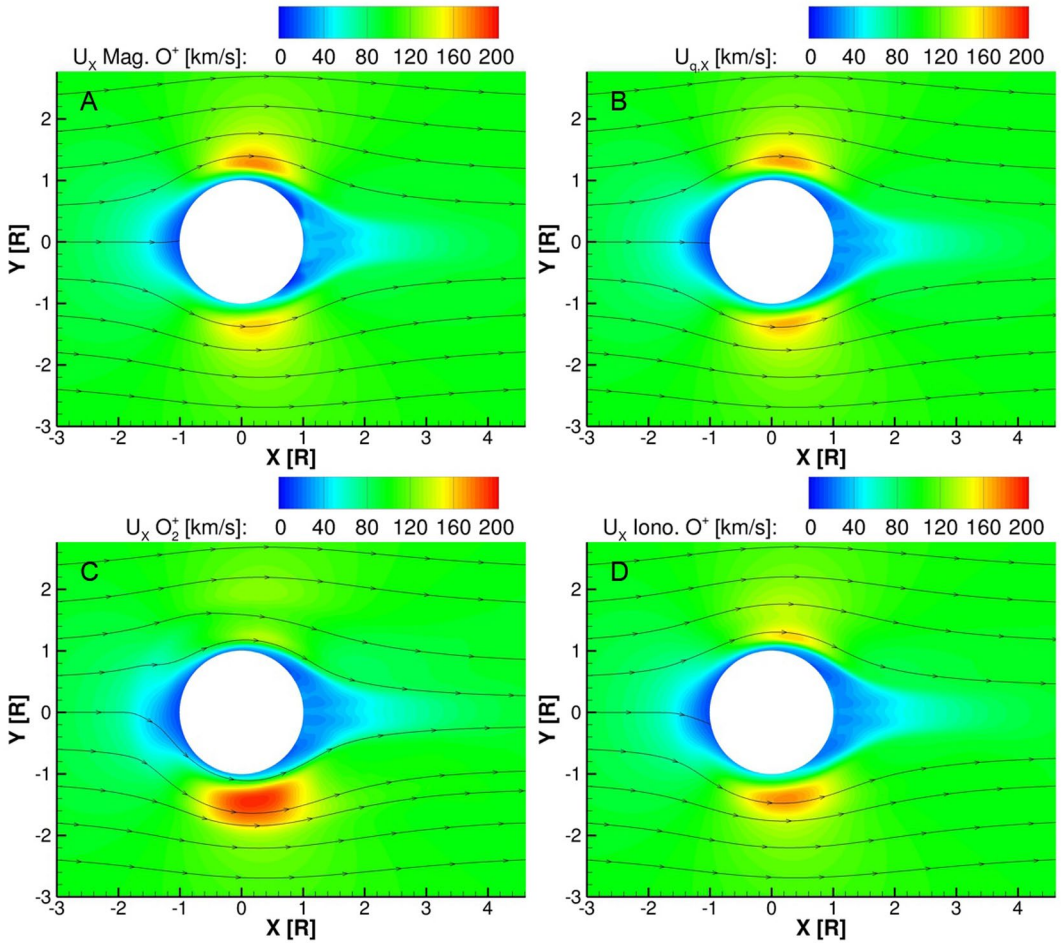

Figure 11. Color contours of the X component of the simulated velocity for each ion fluid (a): magnetospheric O^+; (c): ionospheric O_2^+; (d): ionospheric O^+) and the charge-averaged velocity (b) in the equatorial plane of the case 1, plasma sheet simulation, overlaid with streamlines of the X and Y components of the respective velocities.

the simulations. The electron impact ionization rate depends on the local electron temperature and density. The electron temperature at the outer boundary is fixed at 20 eV in all simulations, and it is cooled similarly throughout the neutral atmosphere in all the simulations. However, the electron density varies with the ion density across the different simulations, as specified by Equation 7. Since the electron impact ionization rate is directly proportional to the electron density, this causes the density of the ionosphere to increase with the density of the ambient plasma.

4. Discussion

The simulations presented in this study illustrate the response of Europa's plasma interaction to the driving of Jupiter's magnetospheric plasma at different locations and for different global states of the magnetosphere. This provides a comprehensive description of how the access of magnetospheric plasma to Europa's surface depends on the external magnetospheric conditions, with important implications for surface sputtering by thermal ions. As described previously, Europa's atmosphere is partially sustained by sputtering of magnetospheric charged particles against Europa's ice (see review by Plainaki et al., 2018). Energetic ions tend to sputter with more productive yields per particle, while thermal ions sputter with lower individual yields but with many more incident particles due to the relatively higher density of thermal ions in Jupiter's magnetosphere (e.g., Cassidy et al., 2013; Vorburger and Wurz, 2018). Our multi-fluid MHD model does not simulate energetic particles, but due to the separation of the magnetospheric O^+ fluid it can describe the precipitation of the thermal plasma that contributes to sputtering. Furthermore, with the previously

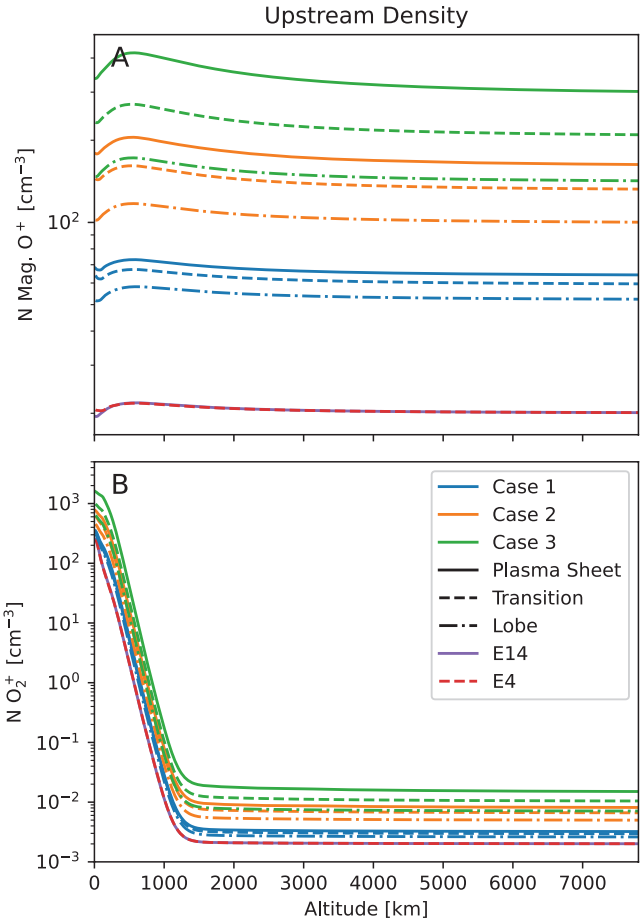

Figure 12. Simulated number densities along the -X axis in all simulations for (a) the magnetospheric O^+ and (b) the ionospheric O_2^+ fluids. Blue lines indicate the Case 1 simulations, orange lines indicate Case 2, and green lines indicate Case 3. Solid lines correspond to the simulations in the plasma sheet configuration (19°S-III longitude), dashed lines to the transitional configuration (76°), and dash-dot lines to the lobe configuration (110°). The flyby simulations are indicated by red dashed lines (E4) and purple solid lines (E14).

described set of simulations we can characterize how thermal plasma precipitation is affected by the electromagnetic fields of the plasma interaction, and how it responds to the range of magnetospheric conditions that Europa experiences.

4.1. Spatial Distribution of Precipitation

To study the precipitation of plasma onto Europa's surface we interpolated the bulk parameters of the ion fluids, including density, velocity, and pressure, from the 3D simulation results to a spherical surface with radius of 1.01 R_{Eu}. We extract parameters at 1.01 R_{Eu}, leaving a buffer of one layer of grid cells above Europa's true surface at 1.0 R_{Eu}, to avoid potential effects from the imposed inner boundary conditions. In the following discussion we use "flux" to refer to the number of ions passing downward through this spherical surface per unit area, per unit time. We calculate the flux for each ion fluid by multiplying the plasma number density with the radial component of the plasma bulk flow velocity. We then use "precipitation rate" to refer to the total number of ions passing downward through the surface per unit time, which we obtain by integrating the above-defined flux of each fluid over the spherical surface area.

In Figure 14 we map the flux of each of the ion fluids from the E4 flyby simulation onto Europa's surface. Cassidy et al. (2013) have previously modeled the flux of magnetospheric plasma to Europa's surface. They traced ions backwards in time from the surface assuming unperturbed incident plasma flow and uniform Jovian magnetospheric magnetic field, and determined that the result should be a circular bulls-eye pattern of flux centered on the trailing hemisphere. By including the plasma interaction fields we find that while the number flux of all three fluids is, similarly, densest over the trailing hemisphere, the bulls-eye pattern is sheared along the direction of the background magnetic field. The direction of the background magnetic field as it maps onto the apexes of Europa's trailing and leading hemispheres is indicated by white arrows in Figure 14. The ionospheric fluids (Figures 14b and 14c) are much denser near the surface than the magnetospheric O^+ fluid (Figure 14a), and they precipitate mainly over the trailing hemisphere. Figure 14a shows the flux of magnetospheric O^+ onto Europa's surface and is overlaid with contours of temperature of the magnetospheric O^+ fluid. We find that the temperature of the magnetospheric O^+ tends to increase near the equator, and the hottest patches of flux (greater than 150 eV) extend from ~240° (West longitude) around to the anti-Jovian meridian (180° West longitude). The temperature of the ionospheric fluids (Figures 14b and 14c) near the surface does not exceed 100 eV except in small patches near the equator at the anti-Jovian meridian.

Figure 15 shows the spatial distribution and temperature of the precipitating magnetospheric O^+ onto Europa's surface in each of the parameter study simulations. We find that the Case 1 simulations, which represent the interaction under high temperature/low density Jovian magnetospheric plasma conditions, exhibit the hottest precipitation, with patches of precipitating plasma hotter than 250 eV over the apex of the anti-Jovian hemisphere. The precipitating magnetospheric O^+ is cooler in Case 2, and cooler still in Case 3 (low temperature/high density conditions). We observe the same trend as the simulations progress within each case from the lobe (where the ambient plasma is sparse and hot) to the plasma sheet (dense and cool). We also observe that the density of precipitating plasma tends to increase in Case 3 relative to Case 1, and in the plasma sheet simulations relative to the lobe simulations.

All of the panels in Figure 15 share common features. We have identified examples of the following features in the bottom-right panel of Figure 15 for the Case 3 plasma sheet simulation with the letters A-D.

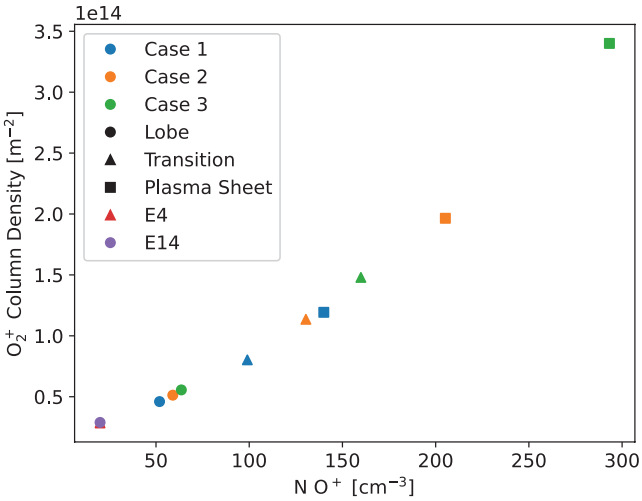

Figure 13. Column densities of Europa's ionosphere along the -X axis in all simulations plotted versus the outer boundary magnetospheric O^+ number density. Blue markers indicate the Case 1 simulations, orange markers indicate Case 2, and green markers indicate Case 3. Circle markers correspond to the simulations in the lobe configuration (19°S-III longitude), triangle markers to the transitional configuration (76°), and square markers to the plasma sheet configuration (110°). The flyby simulations are indicated by a red triangle marker (E4) and a purple circular marker (E14).

Magnetospheric O^+ impinges on the upstream side of the moon, penetrating the ionosphere and reaching the surface to form distorted bullseye patterns centered on 270° longitude (point A). At 90° longitude there are gray patches that we use to indicate that the radial velocity component of the magnetospheric O^+ fluid is directed upward, and therefore no downward plasma precipitation occurred (point B). These patches on the downstream side of the interaction are caused by the curvature of the magnetic field lines at the vertex of the Alfvén wings (see Figure 9). The curved magnetic field geometry leads to currents that flow in the -Y direction; with the mainly southward magnetic field, it exerts a J×B force on all the MHD fluids that causes them to flow away from the surface. Farther downstream the magnetospheric O^+ rejoins the ambient flow, as illustrated in Figures 10 and 11, but due to the low density and speed of magnetospheric O^+ near point B it is a negligible source of plasma.

To the north and south of the patches with no precipitation (point B) there are regions of precipitating magnetospheric O^+ on the leading hemispheres at 90° longitude (points C, D). These plasmas are carried by the flux tubes that convect from the upstream side over Europa in the +X direction due to the prevailing E × B drift. Since Europa's surface and ionosphere do not supply a source of the magnetospheric O^+ ions (see Figure 10a), there are pressure gradients over the leading/downstream hemisphere that point outward, away from Europa's surface. While plasma convects over Europa, the pressure gradients drive the ambient plasma flows toward the surface where the magnetospheric O^+ pressure is low, parallel to the field line direction in the northern hemisphere, and antiparallel in the south. This causes the magnetospheric O^+ to precipitate onto the surface on the leading/downstream side. We note that in the model of Cassidy et al. (2013) the flux of thermal magnetospheric plasma was limited to the trailing hemisphere, causing the sputtering of O_2 to be limited to the trailing hemisphere as well. Our results indicate that due to the plasma interaction some precipitation does occur on the leading/downstream hemisphere, which should contribute to sputtering of O_2 there.

Every simulation exhibited similar features to those identified by points A-D, though as Figure 15 demonstrates these features are of different shapes, densities, and temperatures due to the different upstream plasma conditions in each case.

4.2. Trends in the Total Precipitation Rate

To measure the precipitation rate of thermal magnetospheric ions to Europa's surface we integrated the downward flux of the magnetospheric O^+ fluid over the R = 1.01 R_{Eu} spherical surface. Table 3 reports the total precipitation of magnetospheric O^+ in each simulation. For comparison, Cassidy et al. (2013) assumed a density of 110 cm^{-3}, speed of 76 km/s, and temperature of ~100 eV for the impinging magnetospheric plasma in their model. These parameters are different from the parameters we have used in this study (compare with Table 1), but the results of the Cassidy et al. (2013) study nevertheless provide a useful point of comparison. They found that the precipitation rate of cold magnetospheric oxygen ions to the surface was 40×10^{24} ions/s. In our parameter study simulations the precipitation rate of thermal magnetospheric ions onto the surface ranges from 5.6 to 26×10^{24} ions/s, while for the E4 and E14 flyby simulations the rate is 1.9×10^{24} ions/s and 1.8×10^{24} ions/s, respectively. In our simulations less plasma reaches the surface because most of it is diverted around Europa by the electromagnetic interaction with Europa's ionosphere. We consider the results of Cassidy et al. (2013) to be an upper bound on the precipitation rate due to the un-impeded magnetospheric plasma in their model. Our findings show that when the plasma interaction is considered the flux of magnetospheric plasma to the surface is reduced compared to the result of Cassidy et al. (2013), due to the diversion of the upstream flow by the plasma interaction.

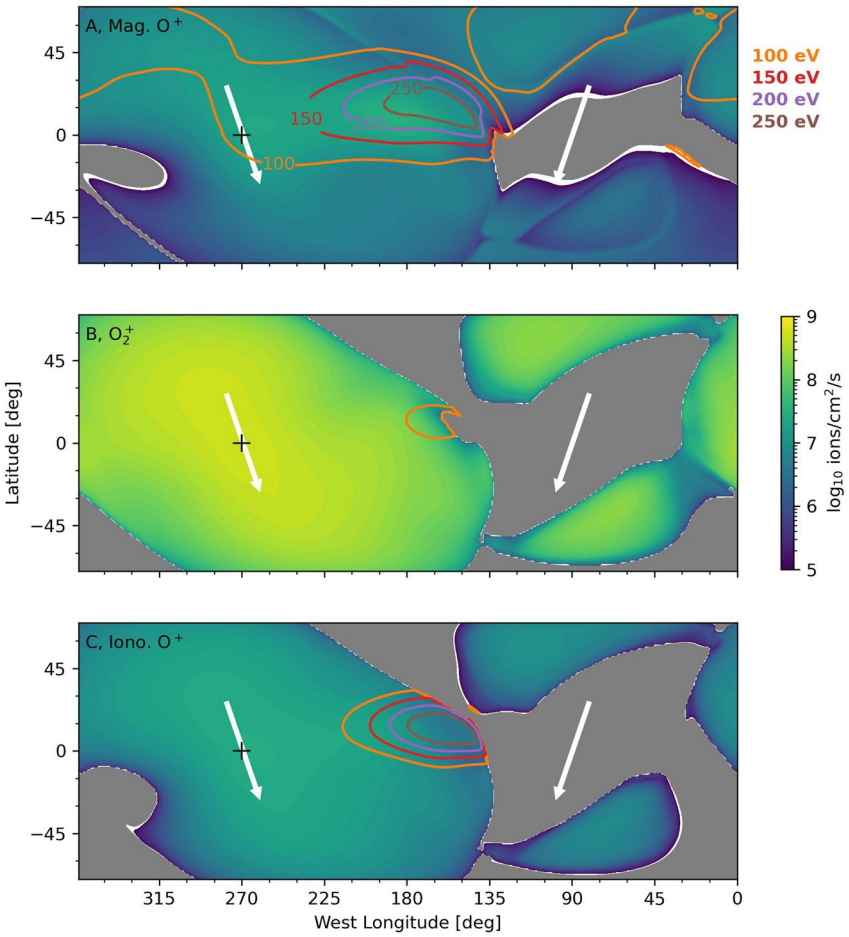

Figure 14. Precipitation of individual ion fluids in the E4 simulation. Each panel shows the spatial distribution of downward ion precipitation to Europa's surface. The surface was extracted at R = 1.01 R_{Eu} (15.6 km altitude) at a resolution of 1 point per degree. Gray regions block out upward-traveling ions, while white regions indicate low density precipitation below the color threshold. Black plus symbols mark the center of the trailing/upstream hemisphere at 270° West Longitude. The center of the anti-Jovian hemisphere is at 180°. White arrows at 270° and 90° longitude show the direction of $B_{I,YZ}$ mapped onto the trailing and leading hemispheres, respectively. In panel A, contour lines indicate the temperature of the precipitating magnetospheric O^+ ions in eV.

Figure 16 shows the total precipitation as a function of magnetic latitude and the upstream, ambient ion density. In Figure 16a we show that for each Case, or state of the global magnetosphere, the precipitation of thermal plasma increases with proximity to the plasma sheet. We also find that the Case 3 (high density/low temperature) simulations see more precipitation than the Case 1 (low density/high temperature) simulations. These trends arise due to the close dependence of precipitation on the upstream ambient plasma density as illustrated by Figure 16b. Since the precipitation of thermal plasma is used as an input to models for Europa's atmosphere (Oza et al., 2019; Teolis et al., 2017; Vorburger and Wurz, 2018), the reduction of this precipitation relative to the upstream flux due to the plasma interaction, and its variability, should be taken into account.

To understand this dependence we investigated the diversion of the upstream flow due to the plasma interaction in these simulations. We seeded uniformly spaced 3D streamlines of magnetospheric O^+ velocity on a disc of 1 R_{Eu} radius upstream of Europa at X = −10 R_{Eu}. We then measured the percentage of streamlines that did not intersect the surface of the moon. If the plasma interaction was not present all the streamlines sourced from the disc would have flowed along straight lines through Europa's surface, and none would be diverted. We found that Europa's plasma interaction diverted 88 ± 2% of the impinging magnetospheric O^+ streamlines around the moon in these simulations. This result is consistent with the previous estimate

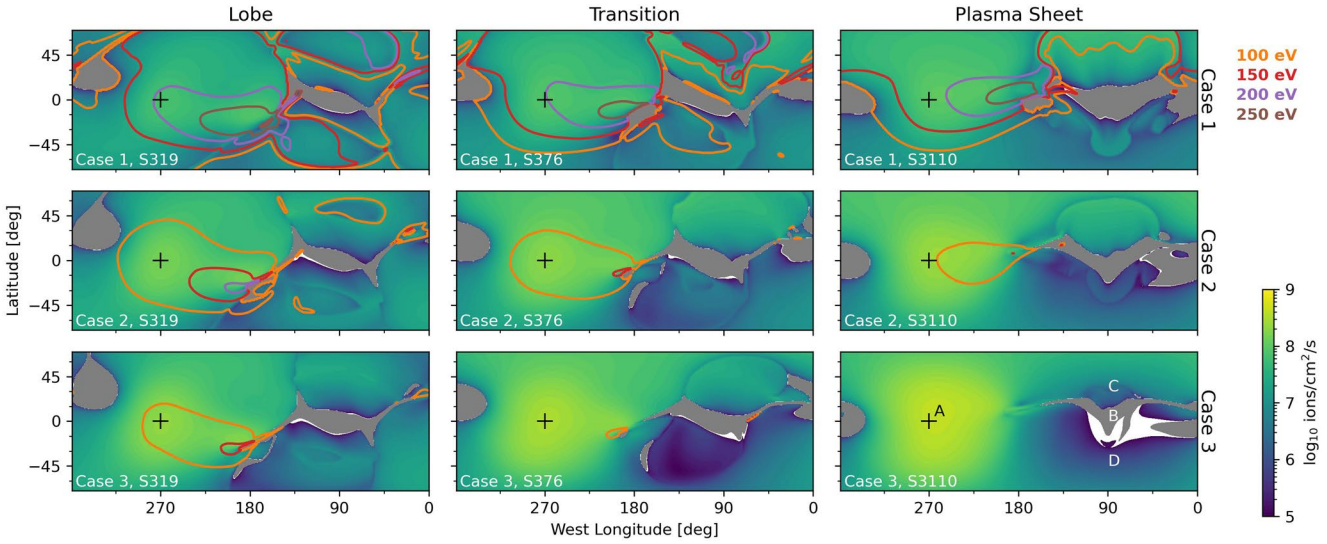

Figure 15. Precipitation of the magnetospheric O^+ fluid in the set of nine parameter study simulations. The format of each panel and the color values are the same as for Figure 14. Columns show simulations of the different magnetospheric states, while rows show the lobe, transition, and plasma sheet simulations for each case.

obtained by Saur et al. (1998) using a neutral atmosphere model with similar column densities. The remaining streamlines reach the surface and the ions streaming along them are counted as precipitation. Since the percentage of diverted streamlines does not vary strongly between the different simulations, the number of precipitating ions is principally controlled by the density of the ambient plasma upstream of Europa.

The consistency of the diversion across all these simulations can be attributed to the feedback loop between the upstream magnetospheric plasma and the ionosphere. When the magnetospheric plasma approaches Europa it may be diverted by the electromagnetic fields of the plasma interaction, but if the magnetospheric plasma is dense enough it will have sufficient momentum to approach Europa's surface where the density of the neutral atmosphere is high. There the magnetospheric plasma will engage in electron impact ionization to produce new ions from Europa's atmosphere. O_2^+ and O^+ ions will be generated at a rate that increases proportionally with the magnetospheric plasma density since the electron impact ionization rate increases with electron density. If the ionosphere had been fixed across all the simulations, the simulations with higher magnetospheric plasma densities and thus more momentum in the magnetospheric plasma would have seen a smaller percentage of diverted streamlines. However, in each simulation the steady-state density of the ionosphere increases with the ambient plasma density due to the dependence of the electron impact ionization rate on the magnetospheric plasma density, as shown in Figure 13. Thus in simulations where the magnetospheric plasma has more momentum due to increased density, the ionosphere density also increases, so that the ionosphere more effectively slows down and diverts the impinging flow. As a result, the percent of diverted streamlines remained approximately constant over all the simulations.

Table 3
Total Magnetospheric O^+ Precipitation Rate [10^{24} Ions/s] in All 11 Simulations

	Lobe	Transition	Plasma sheet
Case 1	5.6	6.6	7.8
Case 2	9.6	13	16
Case 3	13	19	26
Galileo E4 flyby		1.9	
Galileo E14 flyby		1.8	

As an approximation, the magnetospheric ions in our model are assumed to be composed only of O^+. However, S^{2+} ions are also present in Jupiter's magnetospheric plasma at Europa's orbit (Bagenal and Dols, 2020; Kivelson et al., 2004), and while they have the same mass per charge ratio as O^+, S^{2+} ions tend to sputter more effectively due to their higher mass (Vorburger and Wurz, 2018). Since they are omitted in our current model, any sputtering yield estimated from the precipitation rates presented in this work will likely be underestimated. We additionally note that due to the fluid approximation of the model, our MHD simulations do not capture kinetic effects arising from the gyro-motion of individual charged particles or nonMaxwellian plasma distributions, which may have important effects on estimating the sputtering yields due to the space weathering

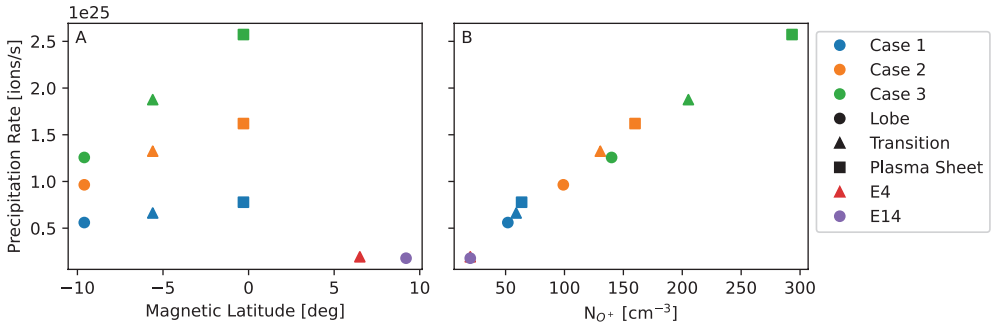

Figure 16. Precipitation rate of magnetospheric O^+ versus (a) magnetic latitude and (b) outer boundary magnetospheric O^+ number density. The markers are organized as in Figure 13.

interaction (Johnson et al., 2009). Therefore, we emphasize that while these results illustrate the range in variability of the precipitation due to external magnetospheric conditions, there are other factors at play that must be accounted for to obtain accurate estimates of sputtering yields.

4.3. Importance of Variations in the Neutral Atmosphere for Precipitation

One element of the plasma interaction which we have not taken into account in this work is the variability of the neutral atmosphere. We selected the parameters of the neutral atmosphere (see Section 2.1.4) for this study based on our model validation efforts using the Galileo E4 and E14 flybys and on previous modeling of the neutral atmosphere. However, it is expected that the density and spatial distribution of the neutral atmosphere will vary with Europa's orbital phase and with Jupiter's synodic period (see review by Plainaki et al., 2018).

Both Plainaki et al. (2013) and Oza et al. (2019) used Monte Carlo simulations to find that solar illumination increases the sputtering yield of atmospheric O_2 by heating Europa's ice, causing the neutral atmosphere to vary periodically with the solar illumination conditions as the moon orbits around Jupiter with a long, 84 h period. They estimated how the density of O_2 and asymmetry of the atmosphere vary as Europa orbits in and out of eclipse, and as the sunlit hemisphere rotates relative to the trailing hemisphere.

As described previously in Section 1, we also anticipate feedback between the neutral atmosphere and the magnetospheric plasma through sputtering. The amount of sputtered neutrals depends in part on the access of the magnetospheric plasma to Europa's surface, which is in turn affected by the strength of the electromagnetic interaction with the ionosphere generated from the neutral atmosphere. A denser neutral atmosphere would tend to generate a denser ionosphere, impeding the precipitation of thermal magnetospheric plasma. Energetic particles also play a significant role in weathering and otherwise altering Europa's icy surface (Paranicas et al., 2001, 2002, 2009, 2000; Nordheim et al., 2018), including producing atmospheric O_2 by sputtering (Cassidy et al., 2013; Vorburger and Wurz, 2018). Though energetic particles are not expected to significantly alter the magnetic fields of the plasma interaction because the total pressure of the ambient environment is dominated by the magnetic field (Kivelson et al., 2004), their contribution to the yield of sputtered neutrals would be necessary to accurately model this coupling between Jupiter's magnetosphere and Europa's atmosphere. While our current model does not include the energetic particle population, their precipitation can be estimated by tracing energetic particles through the electromagnetic fields simulated by the MHD model.

Water plumes may also be an important, small-scale feature of the neutral atmosphere with large-scale implications for the plasma interaction. Recently, Blöcker et al. (2016), Jia et al. (2018), and Arnold et al. (2020) have demonstrated the effects of atmospheric inhomogeneities and plumes on Europa's plasma interaction in MHD and hybrid simulations.

For this study we held the parameters of the neutral atmosphere constant to better focus on the external effects of the magnetosphere on thermal plasma precipitation. However, modeling of the neutral atmosphere has indicated that the density of O_2 varies over time due to various factors, and modeling of the plasma

interaction (in this work and others) has demonstrated that the electromagnetic fields and bulk plasma flows near Europa are closely coupled to the density of the neutral atmosphere. In future work we will model the effects of expected variations in the neutral atmosphere on the plasma interaction.

5. Conclusions

We have extended and refined a multi-fluid MHD model for Europa's plasma interaction, based on the BATS-R-US code, to separately model the bulk properties of Jupiter's magnetospheric plasma (represented by O^+) and the plasmas originating from Europa's atmosphere (O_2^+ and O^+). We have validated the model by simulating the Galileo E4 and E14 flybys and comparing our simulated magnetic fields, plasma density, and plasma velocity to the spacecraft observations. With a favorable data-model comparison, we then used the model to investigate how the large-scale configuration of Europa's plasma interaction and the resulting precipitation of magnetospheric O^+ to Europa's surface respond to the variability of the external plasma and field conditions.

We examined the trends in precipitation and ion temperature as the Jovian magnetospheric conditions change. We found that the precipitation rate of ions increases with the density of the ambient plasma, while similarly the temperature of the precipitation increases with the temperature of the ambient plasma. However, we note that this result does not account for changes in Europa's neutral atmosphere, which is expected to evolve over time in response to changing solar illumination, changing magnetospheric precipitation, and, potentially, water plumes.

We determined that the total precipitation rate of Jupiter's thermal magnetospheric O^+ ions to Europa's surface ranges from (1.8–26) $\times 10^{24}$ ions/s over the parameter space of Jovian magnetospheric conditions that Europa can be expected to experience based on the available observations. These values are significantly smaller than the previous estimate of 40×10^{24} ions/s from the work by Cassidy et al. (2013), which did not include the diversion of the upstream flow due to the plasma interaction. Their result can therefore be considered an upper limit on the precipitation rate.

We conclude that the precipitation of thermal magnetospheric O^+ to Europa's surface is sensitive to changes in the ambient plasma caused by Europa's periodic progression from Jupiter's magnetic lobe to the plasma sheet and back every 11 h, as well as to changes in the global state of the magnetosphere. The most important controlling factor we identified here for the total precipitation rate was the density of the upstream magnetospheric plasma. These changes in magnetospheric conditions alter the plasma interaction, which controls the density, temperature, and spatial distribution of the precipitating magnetospheric plasma onto Europa's surface. In particular, we have found that thermal plasma can precipitate on the leading hemisphere, though the amount is less than on the trailing hemisphere. Since thermal magnetospheric ions are partially responsible for sputtering neutral O_2 out of Europa's ice and into the neutral atmosphere, this variability should be taken into account in models for Europa's neutral atmosphere.

NASA's upcoming Europa Clipper mission (Howell and Pappalardo, 2020) will greatly improve our understanding of Europa's plasma interaction and its coupling to the neutral atmosphere. Europa Clipper will conduct over 40 close flybys of the moon during which the magnetic field and plasma near Europa will be observed simultaneously by the Europa Clipper Magnetometer (ECM) and the Plasma Instrument for Magnetic Sounding (PIMS) investigations. Further, Europa Clipper's Ultraviolet Spectrograph (Europa-UVS) and other in situ instruments (e.g., the MAss SPectrometer for Planetary EXploration/Europa, or MASPEX) will provide new measurements of Europa's neutral atmosphere, better constraining the structure and variability of the atmosphere. Simultaneous observations of the plasma interaction and atmosphere will be critical for supplying input parameters to these simulations, which in turn can provide 3D global context for interpreting the observations. This will enhance the science return of Europa Clipper by illuminating the coupling between the electromagnetic fields, atmosphere, and plasma populations at Europa.

Data Availability Statement

The Galileo Magnetometer data for the Europa flybys were obtained from the NASA Planetary Data System at key GO-J-MAG-3-RDR-HIGHRES-V1.0, DOI 10.17189/1519667. The BATS-R-US code is publicly available for download as a component of the Space Weather Modeling Framework from the Center for Space Environment Modeling at the University of Michigan (http://csem.engin.umich.edu/tools/swmf/).

Acknowledgments
C. D. K. Harris and X. Jia thank the Europa Clipper ECM and PIMS science teams for useful discussions on this work. This work was partially supported by NASA through the Europa Clipper project through contract #1631492 through the Jet Propulsion Laboratory, and contract #143448 through the Applied Physics Laboratory at Johns Hopkins University, and by the Michigan Space Grant Consortium, NASA grant #NNX15AJ20H. High-performance computing resources supporting this work were provided by the NASA High-End Computing (HEC) Program through the NASA Advanced Supercomputing (NAS) Division at Ames Research Center, and the Texas Advanced Computing Center (TACC) at The University of Texas at Austin.

References

Arnold, H., Liuzzo, L., & Simon, S. (2020). Plasma interaction signatures of plumes at Europa. *Journal of Geophysical Research: Space Physics*, *125*, e2019JA027346. https://doi.org/10.1029/2019ja027346

Bagenal, F., & Dols, V. (2020). The space environment of Io and Europa. *Journal of Geophysical Research: Space Physics*, *125*, e2019JA027485. https://doi.org/10.1029/2019ja027485

Bagenal, F., Sidrow, E., Wilson, R. J., Cassidy, T. A., Dols, V., Crary, F. J., et al. (2015). Plasma conditions at Europa's orbit. *Icarus*, *261*, 1–13. https://doi.org/10.1016/j.icarus.2015.07.036

Blöcker, A., Saur, J., & Roth, L. (2016). Europa's plasma interaction with an inhomogeneous atmosphere: Development of Alfvén winglets within the Alfvén wings. *Journal of Geophysical Research: Space Physics*, *121*, 9794–9828. https://doi.org/10.1002/2016ja022479

Breer, B. R., Liuzzo, L., Arnold, H., Andersson, P. N., & Simon, S. (2019). Energetic ion dynamics in the perturbed electromagnetic fields near Europa. *Journal of Geophysical Research: Space Physics*, *124*, 7592–7613. https://doi.org/10.1029/2019ja027147

Cassidy, T. A., Paranicas, C. P., Shirley, J. H., Dalton, J. B. III, Johnson, R. E., Kamp, L., et al. (2013). Magnetospheric ion sputtering and water ice grain size at Europa. *Planetary and Space Science*, *77*, 64–73. https://doi.org/10.1016/j.pss.2012.07.008

Glocer, A., Tóth, G., Ma, Y., Gombosi, T., Zhang, J.-C., & Kistler, L. M. (2009). Multifluid block-adaptive-tree solar wind roe-type upwind scheme: Magnetospheric composition and dynamics during geomagnetic storms-initial results. *Journal of Geophysical Research*, *114*, A12203. https://doi.org/10.1029/2009ja014418

Hall, D. T., Feldman, P. D., McGrath, M. A., & Strobel, D. F. (1998). The far-ultraviolet oxygen airglow of Europa and Ganymede. *The Astrophysical Journal*, *499*(1), 475–481. https://doi.org/10.1086/305604

Hall, D. T., Strobel, D. F., Feldman, P. D., McGrath, M. A., & Weaver, H. A. (1995). Detection of an oxygen atmosphere on Jupiter's moon Europa. *Nature*, *373*(6516), 677–679. https://doi.org/10.1038/373677a0

Howell, S. M., & Pappalardo, R. T. (2020). NASA's Europa clipper-a mission to a potentially habitable ocean world. *Nature Communications*, *11*(1), 1311. https://doi.org/10.1038/s41467-020-15160-9

Jia, X., Kivelson, M. G., Khurana, K. K., & Kurth, W. S. (2018). Evidence of a plume on Europa from Galileo magnetic and plasma wave signatures. *Nature Astronomy*, *2*(6), 459–464. https://doi.org/10.1038/s41550-018-0450-z

Jia, X., Kivelson, M. G., Khurana, K. K., & Walker, R. J. (2010). Magnetic fields of the satellites of Jupiter and Saturn. *Space Science Reviews*, *152*(1–4), 271–305. https://doi.org/10.1007/s11214-009-9507-8

Jia, X., Walker, R. J., Kivelson, M. G., Khurana, K. K., & Linker, J. A. (2009). Properties of Ganymede's magnetosphere inferred from improved three-dimensional MHD simulations. *Journal of Geophysical Research*, *114*, A09209. https://doi.org/10.1029/2009ja014375

Johnson, R. E., Burger, M. H., Cassidy, T. A., Leblanc, F., Marconi, M., & Smyth, W. H. (2009). Composition and detection of Europa's sputter-induced atmosphere. In R. T. Pappalardo, W. B. McKinnon, & K. K. Khurana (Eds.), *Europa (chap. 21)* (pp. 1–780). University of Arizona Press.

Khurana, K. K. (1997). Euler potential models of Jupiter's magnetospheric field. *Journal of Geophysical Research*, *102*(A6), 11295–11306. https://doi.org/10.1029/97ja00563

Khurana, K. K., Kivelson, M. G., Stevenson, D. J., Schubert, G., Russell, C. T., Walker, R. J., & Polanskey, C. (1998). Induced magnetic fields as evidence for subsurface oceans in Europa and Callisto. *Nature*, *395*(6704), 777–780. https://doi.org/10.1038/27394

Kivelson, M. G. (2000). Galileo magnetometer measurements: A stronger case for a subsurface ocean at Europa. *Science*, *289*(5483), 1340–1343. https://doi.org/10.1126/science.289.5483.1340

Kivelson, M. G., Bagenal, F., Kurth, W. S., Neubauer, F. M., Paranicas, C., & Saur, J. (2004). Magnetospheric interactions with satellites. In F. Bagenal, T. E. Dowling, & W. B. McKinnon (Eds.), *Jupiter: The planet, satellites, and magnetosphere (chap. 21)*. Cambridge University Press.

Kivelson, M. G., & Khurana, K. K. (2009). Europa's interaction with the Jovian magnetosphere. In R. T. Pappalardo, W. B. McKinnon, & K. K. Khurana (Eds.), *Europa (chap. 23)*. University of Arizona Press.

Kliore, A. J. (1997). The ionosphere of Europa from Galileo radio occultations. *Science*, *277*(5324), 355–358. https://doi.org/10.1126/science.277.5324.355

Kurth, W. S., Gurnett, D. A., Persoon, A. M., Roux, A., Bolton, S. J., & Alexander, C. J. (2001). The plasma wave environment of Europa. *Planetary and Space Science*, *49*(3), 345–363.(Magnetospheres of the Outer Planets (Part I)). https://doi.org/10.1016/S0032-0633(00)00156-2

Lipatov, A. S., Cooper, J. F., Paterson, W. R., Sittler, E. C. Jr, Hartle, R. E., & Simpson, D. G. (2013). Jovian plasma torus interaction with Europa. Plasma wake structure and effect of inductive magnetic field: 3D hybrid kinetic simulation. *Planetary and Space Science*, *77*, 12–24. https://doi.org/10.1016/j.pss.2013.01.009

McGrath, M. A., Hansen, C. J., & Hendrix, A. R. (2009). Observations of Europa's tenuous atmosphere. In R. T. Pappalardo, W. B. McKinnon, & K. K. Khurana (Eds.), *Europa (chap. 20)*. University of Arizona Press.

Neubauer, F. M. (1998). The sub-Alfvénic interaction of the Galilean satellites with the Jovian magnetosphere. *Journal of Geophysical Research*, *103*(E9), 19843–19866. https://doi.org/10.1029/97je03370

Neubauer, F. M. (1999). Alfvén wings and electromagnetic induction in the interiors: Europa and Callisto. *Journal of Geophysical Research*, *104*(A12), 28671–28684. https://doi.org/10.1029/1999ja900217

Nordheim, T. A., Hand, K. P., & Paranicas, C. (2018). Preservation of potential biosignatures in the shallow subsurface of Europa. *Nature Astronomy*, *2*(8), 673–679. https://doi.org/10.1038/s41550-018-0499-8

Oza, A. V., Leblanc, F., Johnson, R. E., Schmidt, C., Leclercq, L., Cassidy, T. A.,& Chaufray, J.-Y. (2019). Dusk over dawn O2 asymmetry in Europa's near-surface atmosphere. *Planetary and Space Science*, *167*, 23–32. https://doi.org/10.1016/j.pss.2019.01.006

Paranicas, C., Carlson, R. W., & Johnson, R. E. (2001). Electron bombardment of Europa. *Geophysical Research Letters*, *28*(4), 673–676. https://doi.org/10.1029/2000gl01232010.1029/2000gl012320

Paranicas, C., Cooper, J. F., Garrett, H. B., Johnson, R. E., & Sturner, S. J. (2009). Europa's radiation environment and its effects on the surface. In R. T. Pappalardo, W. B. McKinnon, & K. K. Khurana (Eds.), *Europa (chap. 22)*. University of Arizona Press.

Paranicas, C., McEntire, R. W., Cheng, A. F., Lagg, A., & Williams, D. J. (2000). Energetic charged particles near Europa. *Journal of Geophysical Research*, *105*(A7), 16005–16015. https://doi.org/10.1029/1999ja000350

Paranicas, C., Ratliff, J. M., Mauk, B. H., Cohen, C., & Johnson, R. E. (2002). The ion environment near Europa and its role in surface energetics. *Geophysical Research Letters*, *29*(5), 18-1-18-4. https://doi.org/10.1029/2001gl014127

Paterson, W. R., Frank, L. A., & Ackerson, K. L. (1999). Galileo plasma observations at Europa: Ion energy spectra and moments. *Journal of Geophysical Research*, *104*(A10), 22779–22791. https://doi.org/10.1029/1999ja900191

Plainaki, C., Cassidy, T. A., Shematovich, V. I., Milillo, A., Wurz, P., Vorburger, A., et al. (2018). Toward a global unified model of Europa's tenuous atmosphere. *Space Science Reviews*, *214*(1). https://doi.org/10.1007/s11214-018-0469-6

Plainaki, C., Milillo, A., Mura, A., Saur, J., Orsini, S., & Massetti, S. (2013). Exospheric O2 densities at Europa during different orbital phases. *Planetary and Space Science*, *88*, 42–52. https://doi.org/10.1016/j.pss.2013.08.011

Pospieszalska, M. K., & Johnson, R. E. (1989). Magnetospheric ion bombardment profiles of satellites: Europa and Dione. *Icarus*, *78*(1), 1–13. https://doi.org/10.1016/0019-1035(89)90065-1

Rubin, M., Jia, X., Altwegg, K., Combi, M. R., Daldorff, L. K. S., Gombosi, T. I., et al. (2015). Self-consistent multifluid MHD simulations of Europa's exospheric interaction with Jupiter's magnetosphere. *Journal of Geophysical Research: Space Physics*, *120*, 3503–3524. https://doi.org/10.1002/2015ja021149

Rubin, M., Koenders, C., Altwegg, K., Combi, M. R., Glassmeier, K.-H., Gombosi, T. I., et al. (2014). Plasma environment of a weak comet - Predictions for Comet 67P/Churyumov-Gerasimenko from multifluid-MHD and Hybrid models. *Icarus*, *242*, 38–49. https://doi.org/10.1016/j.icarus.2014.07.021

Saur, J., Strobel, D. F., & Neubauer, F. M. (1998). Interaction of the Jovian magnetosphere with Europa: Constraints on the neutral atmosphere. *Journal of Geophysical Research*, *103*(E9), 19947–19962. https://doi.org/10.1029/97je03556

Schilling, N. (2006). *Time varying interaction of Europa's atmosphere-ionosphere and it's conducting ocean with the Jovian magnetosphere (Unpublished doctoral dissertation)*. University of Cologne. https://doi.org/10.1515/9783110927375

Schilling, N., Neubauer, F. M., & Saur, J. (2008). Influence of the internally induced magnetic field on the plasma interaction of Europa. *Journal of Geophysical Research*, *113*, A03203. https://doi.org/10.1029/2007ja012842

Teolis, B. D., Wyrick, D. Y., Bouquet, A., Magee, B. A., & Waite, J. H. (2017). Plume and surface feature structure and compositional effects on Europa's global exosphere: Preliminary Europa mission predictions. *Icarus*, *284*, 18–29. https://doi.org/10.1016/j.icarus.2016.10.027

Tóth, G., van der Holst, B., Sokolov, I. V., De Zeeuw, D. L., Gombosi, T. I., Fang, F., et al. (2012). Adaptive numerical algorithms in space weather modeling. *Journal of Computational Physics*, *231*(3), 870–903. https://doi.org/10.1016/j.jcp.2011.02.006

Volwerk, M., Khurana, K., & Kivelson, M. (2007). Europa's Alfvén wing: Shrinkage and displacement influenced by an induced magnetic field. *Annales Geophysicae*, *25*(4), 905–914. https://doi.org/10.5194/angeo-25-905-2007

Vorburger, A., & Wurz, P. (2018). Europa's ice-related atmosphere: The sputter contribution. *Icarus*, *311*, 135–145. https://doi.org/10.1016/j.icarus.2018.03.022

Zimmer, C. (2000). Subsurface oceans on Europa and Callisto: Constraints from Galileo magnetometer observations. *Icarus*, *147*(2), 329–347. https://doi.org/10.1006/icar.2000.6456